

1

2 ASYMMETRIC EXPRESSION OF ARGONAUTES IN ARABIDOPSIS  
3 REPRODUCTIVE TISSUES

4

5

6 Jullien PE<sup>1,2\*</sup>, Bonnet DMV<sup>1</sup>, Pumplin N<sup>2</sup>, Schroeder JA<sup>1</sup>, and Voinnet O<sup>2</sup>

7

8 <sup>1</sup> Institute of Plant Sciences, University of Bern, Bern, Switzerland.

9 <sup>2</sup> Institute of Molecular Plant Biology, Swiss Federal Institute of Technology Zurich (ETH-  
10 Zurich), Zurich, Switzerland.

11

12 AUTHOR ORCID IDs:

13 Pauline E. Jullien (#0000-0003-1212-3246)

14 FOR CORRESPONDENCE:

15 Pauline E. Jullien ([pauline.jullien@ips.unibe.ch](mailto:pauline.jullien@ips.unibe.ch))

16

17 Running title: Argonautes during reproduction

18 Key words: Argonautes, reproduction, Arabidopsis, Gametes, endosperm, embryo

19

20 ABSTRACT

21 During sexual reproduction, development of a totipotent zygote from the fusion of highly  
22 differentiated gametes is accompanied by a dynamic regulation of gene expression. This  
23 notably involves RNA silencing operated by Argonautes (AGO) effector proteins. While  
24 AGOs' roles during *Arabidopsis* somatic life have been extensively investigated, less is known  
25 about their expression during reproduction, which proceeds via double-fertilization of an egg  
26 and a central cell, leading respectively to the embryo and a supportive tissue known as  
27 endosperm. Using full-locus translational reporters for all ten *Arabidopsis* AGOs, we uncover  
28 cell-specific expression patterns and AGO-intrinsic subcellular localizations in reproductive  
29 tissues. However, while some *Arabidopsis* AGOs are enriched in both male and female  
30 gametes, *i.e.* sperm and egg cells, they are comparably low-expressed in accessory, *i.e.*  
31 vegetative and central cells. Likewise, following fertilization, several AGOs are expressed in  
32 the early embryo, yet below detection in the early endosperm. Thus, there is pre- and post-  
33 fertilization asymmetry between the embryo and endosperm lineages. Later during embryo  
34 development, AGO9, AGO5 and AGO7 are restricted to the apical embryonic meristem in  
35 contrast to AGO1, AGO4, AGO6 and AGO10. Beside shedding some light onto *Arabidopsis*  
36 reproduction, the plant material generated here should constitute a valuable asset to the RNA  
37 silencing community by enabling functional AGOs studies.

38

39

40

41

42

## 43 INTRODUCTION

44 In most eukaryotes, sexual reproduction involves specialized cellular structures and entails  
45 complex orchestration of the timing and spatial localization of gene expression. In the model  
46 plant *Arabidopsis*, reproduction involves the development of a haploid structure called  
47 gametophyte in both male and female reproductive organs. The mature male gametophyte, or  
48 pollen grain, contains three cells: one vegetative cell and two gametes known as sperm cells.  
49 The mature female gametophyte, on the other hand, contains seven cells: three antipodal cells  
50 of unknown function, two synergides involved in pollen tube reception and guidance, one  
51 central cell and one egg cell. Fertilization of the egg cell by one of the sperm cells forms the  
52 embryo proper that will later develop into the next-generation plant. Fertilization of the  
53 homodiploid central cell by the second sperm cell forms the endosperm, a nourishing tissue  
54 required for proper seed development. In addition, the female gametophyte as well as the  
55 developing endosperm and embryo are surrounded by 4 layers of maternal integuments  
56 connected to the mother plant's vasculature at the chalazal pole.

57 Small RNAs (sRNA) are key regulators of gene expression. Their importance during sexual  
58 reproduction has been highlighted by the discovery of a class of reproduction-specific sRNA  
59 known as Piwi-interacting RNAs (piRNAs) in animals (Castel and Martienssen, 2013; Weick  
60 and Miska, 2014). Likewise, the importance of reproduction-specific small RNAs has also been  
61 recognized in plants (Mosher and Melnyk, 2010; Van Ex et al., 2011). Beyond the roles of  
62 microRNAs (miRNAs) in embryonic development, small interfering (si)RNA tame transposon  
63 in the pollen (Slotkin et al., 2009) and during ovule development (Olmedo-Monfil et al., 2010)  
64 but also could be linked to hybrid lethality as they were shown to be involved the regulation of  
65 parental genome dosage (Borges et al., 2018; Martinez et al., 2018). RNA silencing in plants  
66 can be divided into Post-Transcriptional Gene Silencing (PTGS) and Transcriptional Gene  
67 Silencing (TGS). Both pathways rely on the generation of small (s)RNAs of 21, 22 or 24  
68 nucleotides in length by DICER-LIKE enzymes, of which there are four paralogs in  
69 *Arabidopsis* (DCL1-4). These sRNA execute PTGS or TGS upon their loading into  
70 ARGONAUTE (AGO) effector proteins. Despite the established impact of sRNA-pathway  
71 mutations in plant biology, little is known of the expression profiles of silencing-pathway  
72 proteins in reproductive and post-reproductive tissues. In particular, the cell-specific  
73 expression and subcellular localization patterns of AGOs remain largely unknown.

74 The *Arabidopsis* genome encodes ten AGO genes divided into three phylogenetic clades  
75 (Mallory and Vaucheret, 2010) conserved among flowering plants (Fang and Qi, 2015; Zhang  
76 et al., 2015). Clade I consist of AGO1/5/10, with AGO1 being the ubiquitously-expressed  
77 member. *ago1* mutants display aberrant sporophytic phenotypes likely due to AGO1's key role  
78 in executing miRNA functions. Embryonic *ago1* mutant phenotypes were only observed,  
79 however, from the torpedo stage (Lynn et al., 1999). The second clade I member, AGO10, has  
80 been implicated in the control of shoot apical meristem (SAM) identity from late stages of  
81 embryo development (Lynn et al., 1999; Moussian et al., 1998), despite being expressed from  
82 very early stages (Tucker et al., 2008). In fact, early embryo phenotypes were only observed  
83 in the double *ago1ago10* mutant, thereby suggesting functional redundancy between the two  
84 proteins at this stage, possibly in executing miRNA-directed silencing. Supporting this notion,  
85 early embryo phenotypes are observed in *dcl1* mutants exhibiting compromised miRNA  
86 processing (Nodine and Bartel, 2010; Seefried et al., 2014; Willmann et al., 2011). Contrasting  
87 with that of AGO1 and AGO10, AGO5 expression is substantially enriched in reproductive  
88 tissues (Tucker et al., 2012). A dominant AGO5 allele (*ago5-4*) arrests female gametophyte  
89 development altogether (Tucker et al., 2012) while *ago5* recessive mutants display early  
90 flowering (Roussin-Léveillé et al., 2020).

91 The AGO Clade II is constituted of AGO7, AGO2 and AGO3. AGO7 has a well-established  
92 role in leaf development yet no overt function in reproductive tissues has been describe thus  
93 far. Despite AGO2 and AGO3 displaying higher expression levels in reproductive tissue, their  
94 role(s) during reproduction remains, likewise, elusive because no developmental phenotypes  
95 were observed (Jullien et al., 2018). Clade III includes AGO4/6/9/8, which, with the exception  
96 of the truncated AGO8 (Takeda et al., 2008), have all been implicated in DNA methylation  
97 commonly referred as the RNA-dependent-DNA-methylation (RdDM) pathway (Matzke and  
98 Mosher, 2014). The RdDM pathway is required for the establishment of new DNA methylation  
99 pattern as well as the maintenance of cytosine methylation in the CHH context. AGO4 and  
100 AGO6 are mostly ubiquitously expressed, whereas AGO8 and AGO9 seem specific for  
101 reproductive tissue (Havecker et al., 2010; Olmedo-Monfil et al., 2010; Wuest et al., 2010). In  
102 particular, AGO9 is involved in meiosis, megaspore mother cell differentiation and transposon  
103 silencing in the egg cell (Oliver et al., 2014; Olmedo-Monfil et al., 2010). Megaspore mother  
104 cell differentiation is also impeded in *ago4*, *ago6* and *ago8* mutants (Hernández-Lagana et al.,  
105 2016) suggesting an important role for RdDM during this process.

106 To help deciphering the roles of sRNA pathways in reproductive processes, we have generated  
107 stable transgenic lines expressing full length fluorescently tagged AGOs under their cognate  
108 endogenous promoter and analyzed their expression as well as intracellular localization in  
109 reproductive tissues.

## 110 RESULTS AND DISCUSSION

### 111 ARGONAUTES TRANSLATIONAL REPORTERS

112 In order to investigate the expression pattern and intracellular localization of the ten  
113 *Arabidopsis* AGO proteins, we generated full-locus reporter constructs in which the open  
114 reading frames (ORFs) of fluorescent proteins were fused to each AGO coding sequence in  
115 their genomic contexts, using multiple Gateway™ cloning. We engineered N-terminal  
116 translational fusions, since N-terminal, but not C-terminal, tagging preserves *Arabidopsis*  
117 AGOs' functionality (Carbonell et al., 2012). Each AGO construct was cloned under the  
118 corresponding presumptive promoter (1.3kb to 2.5kb upstream start codons) and terminators  
119 (467bp to 1kb downstream of stop codons). This generated pAGO:FP-AGO constructs, where  
120 "FP" corresponds to either the Green Fluorescent Protein (GFP) or mCherry (mCh). For the  
121 sake of simplification, the constructs will be referred to FP-AGOX (where X is the number of  
122 each AGO1-10) in the main text and FPX in the figures. For example, pAGO1:mCherry-AGO1  
123 will be shortened to mCherry-AGO1 in the main text and to mCh1 in figures. Construct were  
124 transformed in their respective mutant background, at least 6 T1 were screened for each  
125 construct and all show a consistent expression pattern in the tissue examined. A detail map of  
126 the constructs can be found in Fig. S1 and a summary of their expression pattern in Fig.S11.  
127 Functional complementation was validated for AGO1, AGO4, AGO5, AGO6 and AGO7 and  
128 can be found in Fig. S2, Fig. S3, Fig. S4, Fig. S5 and Fig. S6 respectively.

### 129 AGO EXPRESSION PATTERNS IN THE MATURE FEMALE GAMETOPHYTE

130 To gain insights into AGO protein expression patterns in the mature female gametophyte, we  
131 analyzed fluorescent signals of each protein fusion, using confocal microscopy. Almost all  
132 AGOs accumulate in the mature female gametophyte (Fig. 1A-K) except GFP-AGO10 (Fig.  
133 1D) and mCherry-AGO3 (Fig. 1J), which are only detected in the maternal integument. The  
134 clade I mCherry-AGO1 and mCherry-AGO5 reporters display similar accumulation patterns  
135 in the female gametophyte (Fig. 1B-C). They are mainly detected in the egg cell and, to a lower  
136 extent, in the central cell. mCherry-AGO1 and mCherry-AGO5 also accumulate in the maternal

137 integument with mCherry-AGO1 being detected in both the inner and outer integument, and  
138 mCherry-AGO5 solely in the former, as previously reported (Tucker et al., 2012). Both  
139 mCherry-AGO1 and mCherry-AGO5 signals are particularly pronounced in the nucellus at the  
140 chalazal pole of the ovule. Clade I, GFP-AGO10 mainly accumulates in the inner-integument  
141 of the ovule with a stronger signal at the chalazal seed coat and in vascular tissues of the  
142 funiculus (Fig. 1D, Fig. S7A-B).

143 The main clade III *i.e.* RdDM AGO's, mCherry-AGO4 and mCherry-AGO6, accumulate  
144 ubiquitously in both integuments and female gametophyte, with stronger signals in the egg cell  
145 (Fig. 1E-F). The reproduction-stage-specific RdDM AGO's, mCherry-AGO9 and mCherry-  
146 AGO8, show more spatially restricted expression patterns (Fig. 1G-H). mCherry-AGO9  
147 accumulates mainly in the egg cell within the female gametophyte but can be detected, albeit  
148 at lower levels, in the central cell. Strong mCherry-AGO9 accumulation is also detected in the  
149 nucellus and funiculus (Figure 1H and Fig. S8A), consistent, for the latter, with previous *in situ*  
150 hybridization results (Olmedo-Monfil et al., 2010). mCherry-AGO8 is specifically detected in  
151 the mature egg cell (Fig. 1G). Egg cell expression of both AGO8 and AGO9 is supported by  
152 conclusions drawn from transcriptional fusions for both AGO9 and AGO8 (Sprunck et al.,  
153 2019) as well as transcriptomic data (Fig. S9B, (Wuest et al., 2010)). However, mCherry-  
154 AGO9 protein fusion expression in the egg cell do not agree with previously published results  
155 obtained by immuno-fluorescence (Olmedo-Monfil et al., 2010). Like mCherry-AGO8, the  
156 clade II-member mCherry-AGO2 is also specifically detected in the egg cell (Fig. 1I) while  
157 clade II-member mCherry-AGO3 is solely detected in the chalazal seed coat of the ovule (Fig.  
158 1J, (Jullien et al., 2018)). The last clade II-member, GFP-AGO7, is detected in all cell types of  
159 the female gametophyte and surrounding integument, with significant enrichment in the egg  
160 cell, similarly to AGO1 (clade I), AGO4 and AGO6 (clade III) (Fig. 1K).

161 Overall, our analysis shows that all ten *Arabidopsis* AGOs are detected in mature ovules before  
162 fertilization. Within the female gametophyte their accumulation seems to be particularly  
163 enriched in the egg cell compared to the central cell. Preferential AGO expression in the egg  
164 cell was confirmed using previously published female gametophyte transcriptome data  
165 obtained after laser-capture microdissection (Fig. S9A, (Wuest et al., 2010)). Our data together  
166 with the potential *ago8* phenotype during MMC development (Hernández-Lagana et al., 2016)  
167 suggest that AGO8 might not be a pseudogene. AGO8 was thought to be a pseudogene as it  
168 possesses a premature stop codon predicted to result in a truncated protein containing a PAZ  
169 domain but not the catalytically active PIWI domain (Takeda et al., 2008). Our observation of

170 mCherry-AGO8 protein specifically in the egg cell (Fig. 1G) could result from the  
171 accumulation of a truncated mCherry-AGO8 protein in this particular cell type. However, we  
172 could not test this hypothesis using Western blot due to the very low expression of mCherry-  
173 AGO8. It is nevertheless tempting to hypothesis that a truncated AGO8 protein could act as a  
174 dominant negative sRNA regulator specifically in the egg cell as it was shown for the dominant  
175 *ago5-4* allele that similarly express a truncated AGO5 including the PAZ but not the PIWI  
176 domain (Tucker et al., 2012). Together our results suggest a complex regulation of sRNA  
177 loading and function in the egg cell.

#### 178 **AGO EXPRESSION PATTERNS IN THE MALE GAMETOPHYTE**

179 Analysis of the translational reporters in mature pollen grain (Fig. 2A-H) revealed a preferential  
180 enrichment of some AGOs in sperm cells. Indeed, mCherry-AGO1, mCherry-AGO2, GFP-  
181 AGO7, mCherry-AGO4 and mCherry-AGO9 were solely detected in those cells (Fig. 2 B, D,F-  
182 H). mCherry-AGO5 and mCherry-AGO6 where mainly detected in sperm cells, but also in the  
183 vegetative cell, albeit only at substantially lower levels (Fig. 2 C, E). AGO5 sperm cell  
184 expression was previously reported (Borges et al., 2011; Tucker et al., 2012).The mCherry-  
185 AGO3, mCherry-AGO8 and GFP-AGO10 reporters signals are not detected in mature pollen.

186 In order to address if paternally-expressed AGOs could be potentially transmitted during  
187 fertilization, we investigated the presence of the protein fluorescent signals in germinated  
188 pollen (Fig. 2I-P). All AGOs showing expression in sperm cells were indeed also detected in  
189 germinated pollen, suggesting that AGO-loaded sRNAs of paternal origin could be transported  
190 to the egg cell and potentially regulate gene expression in the zygote at, or shortly after,  
191 fertilization. Such phenomena are now proven to be important for embryonic development in  
192 mammals (Conine et al., 2018; Sharma et al., 2018; Yuan et al., 2016). Data highlighting such  
193 phenomena are rare in *Arabidopsis*. Indeed, most mutants affecting embryo development are  
194 rather sporophytic recessive rather than showing a paternal gametophytic effect (Meinke, 2020)  
195 which is the case for mutants affecting DCL1 the main micro RNA processing enzyme in  
196 *Arabidopsis* (Nodine and Bartel, 2010). However, recently, a microRNA mutant for miR159  
197 was found to have a paternal effect on endosperm development via the downregulation of the  
198 MYB33 transcription factor (Zhao et al., 2018b). The high expression of miR159 in sperm cell  
199 as well as the very early nature of the observed phenotype suggest that miR159 could be  
200 delivered paternally at fertilization.

#### 201 **AGO EXPRESSION PATTERNS IN THE EARLY SEED**

202 To gain insights into AGO accumulation during early seed development, we observed  
203 fluorescent signals in seeds at one Day-After-Pollination (1 DAP), using confocal microscopy  
204 (Fig. 3A-I). At this stage, we could detect expression of eight out of ten *Arabidopsis* AGOs,  
205 while signals from mCherry-AGO2 and mCherry-AGO8 were below detection limit. Clade I  
206 mCherry-AGO1 is detected in both inner and outer integument layers in the sporophytic tissue  
207 as well as in the embryo, but is below detection in the endosperm (Fig. 3A). Similarly, clade I  
208 mCherry-AGO5 is detected in the embryo and inner (but not outer) integument, while it is  
209 excluded from the endosperm (Fig. 3B). Despite not being detected in the egg cell, clade I  
210 GFP-AGO10 could be detected in the early embryo but not in the endosperm (Fig. 3C). Strong  
211 GFP-AGO10 accumulation is also observed in the funiculus' vasculature and the seed/ovule  
212 vascular termination (Fig. S7). As previously described, accumulation of the clade II mCherry-  
213 AGO3 is limited to the chalazal seed coat (Fig. 3H; (Jullien et al., 2018)). Clade II GFP-AGO7  
214 is detected in all cell types except the endosperm, and its accumulation is particularly strong in  
215 the chalazal seed coat (Fig. 3I).

216 Among the clade II AGOs involved in RdDM, mCherry-AGO4 shows the strongest  
217 accumulation, especially in the sporophytic tissues (Fig. 3D). mCherry-AGO4 can be detected  
218 in the early embryo (Fig 3E) but is not detected in the endosperm. The expression pattern of  
219 mCherry-AGO6 is similar to that of mCherry-AGO4 (Fig.3F), although the signal is of lower  
220 intensity. This result agrees with the known redundancy of AGO4 and AGO6 in mediating  
221 DNA methylation and TGS at some genetic loci (Stroud et al., 2012; Zheng et al., 2007).  
222 mCherry-AGO9 could be detected in the embryo and also in the endosperm, although not in  
223 the integuments (Fig. 3G). In fact, mCherry-AGO9, is visible from the first nuclear division of  
224 the endosperm, upon which its signal decreases in intensity but it is still detected at the 4-cells  
225 embryo stage (Fig. 3G and Fig. S8B-C). Based on our reporter constructs, AGO9 appears as  
226 the only AGO detected during endosperm development.

227 To conclude, we observed a strong asymmetry of AGOs' patterns between the endosperm and  
228 the embryonic lineages. This difference is supported by LCM transcriptomic data from  
229 developing seeds (Fig. S8) and suggests a much less active involvement of RNA silencing  
230 pathways in the endosperm compared to the embryo, during early seed development. In  
231 *Arabidopsis*, the RdDM pathway is responsible for Cytosine DNA methylation in the CHH  
232 context. It relies on the constant *denovo* DNA methylation by the *de novo* DNA  
233 methyltransferases (DRM1 and DRM2) and loading of sRNA by Class II AGOs. In the case of  
234 of Class II AGOs similarly to what was observed with the *de novo* DNA methyltransferases



235 (Jullien et al., 2012), the asymmetry of expression observed between embryo and endosperm  
236 lineage could contribute to the high CHH methylation observed during embryo development  
237 compared to the endosperm (Bouyer et al., 2017; Gehring et al., 2009; Hsieh et al., 2009;  
238 Kawakatsu et al., 2017).

#### 239 **AGO EXPRESSION PATTERNS IN HEART-STAGE EMBRYO**

240 In order to investigate AGO accumulation patterns in the differentiated zygote, we dissected  
241 heart-stage embryos where most early developmental decision already took place and  
242 performed confocal imaging using the fluorescently tagged AGO transgenic lines (Fig. 4A-H).  
243 As previously reported (Du et al., 2019; Lynn et al., 1999), clade I mCherry-AGO1 is expressed  
244 in all cells of the heart-stage embryo (Fig. 4B). Similarly, we observed a ubiquitous expression  
245 of the clade II mCherry-AGO4 and mCherry-AGO6 (Fig. 4E-F). By contrast, clade III  
246 mCherry-AGO2, mCherry-AGO3 and clade II mCherry-AGO8 are could not be detected in  
247 the heart-stage embryo. Clade I GFP-AGO10 displays its previously reported pattern (Du et  
248 al., 2019; Tucker et al., 2008), with fluorescent signals observed in the adaxial part of  
249 cotyledons and in the pre-vasculature (Fig 4D).

250 The three remaining AGOs, AGO5 (clade I), AGO9 (clade III) and AGO7 (clade II)  
251 accumulate specifically in the shoot apical meristem region (SAM) of the heart-stage embryo  
252 (Fig. 4C, G, H), a pattern already documented for AGO5 using a YFP fluorescent reporter  
253 (Tucker et al., 2012). In agreement with our results, AGO5, AGO7 and AGO9 transcript were  
254 found to be enriched in meristematic stem cell both at the embryonic and adult stage (Gutzat  
255 et al., 2018). Although AGO7 and AGO9 function in meristem remain to be investigated, recent  
256 work from Roussin-Leveillee *et al* suggest that AGO5 function in the meristem is involved in  
257 regulating flowering (Roussin-Léveillé et al., 2020). Indeed, *ago5* mutant display an early  
258 flowering phenotype but do not affect leaf morphology (Fig.S4, (Roussin-Léveillé et al.,  
259 2020)). It is thought to do so by interacting with miR156 leading to the repression of SPL  
260 transcription factors. However miR156 was shown to affect both flowering and leaf  
261 morphology (Wu et al., 2009) which suggest a more complex regulation of this pathway  
262 possibility via differential AGO loading and function of miR156 or miR157 isoform (Ebhardt  
263 et al., 2010; He et al., 2018) in meristematic region.

#### 264 **AGO INTRACELLULAR LOCALIZATION PATTERNS**

265 *Arabidopsis* AGO1 and AGO4 have been shown to shuttle between the cytoplasm and the  
266 nucleus although their steady-state subcellular localizations seem to reflect their involvement  
267 in either PTGS (clade I and II) and TGS/RdDM (Clade III), respectively: AGO1 is mostly

268 cytoplasmic and AGO4 nuclear (Bologna et al., 2018; Ye et al., 2012). In agreement with their  
269 involvement in Clade I and II, mCherry-AGO1, mCherry-AGO5, mCherry-AGO2, mCherry-  
270 AGO3, GFP-AGO10 are mostly localized in the cytoplasm in reproductive cells (Fig. 1B-D,  
271 Fig. 1I-J, Fig. 3A-C, Fig. 3H, Fig. 4B-D). However, we observed that mCherry-AGO1, mCherry-  
272 AGO5, mCherry-AGO2 form cytosolic aggregates that were observed in only certain cell types  
273 such as the nucellus and sperm cells (Fig. 1B-C and Fig. 2B-C, G). However, caution should  
274 be exerted in interpreting these observations given that artefactual aggregation has been  
275 reported with mCherry-tagged proteins (Cranfill et al., 2016; Landgraf et al., 2012). It is likely  
276 that these AGO foci occur in tissues where AGO1, AGO5 and AGO2 are particularly highly  
277 expressed. Further work is required to assess if the mCherry-AGO1, mCherry-AGO5, and  
278 mCherry-AGO2 aggregates represent relevant biological entities.

279 The main Clade II AGOs, mCherry-AGO4 and mCherry-AGO6, are localized in the nucleus  
280 in all reproductive cell types analyzed (Fig. 1E-F, Fig. 2D-E, Fig. 3D-F, Fig. 4E-F).  
281 Occasionally, cytoplasmic localization could be observed in the ovule integument or embryo  
282 likely due to disruption of the nuclear membrane during cell division. Nuclear localization for  
283 AGO4 and AGO6 was previously observed in other tissues (Ye et al., 2012; Zheng et al., 2007).  
284 Perhaps more strikingly, mCherry-AGO9 displays nuclear localization in somatic tissues (Fig.  
285 1H, Fig. 3G, Fig. 4G, Fig. S8) but appears to be also partially localized to the cytoplasm in the  
286 central and egg cells (Fig. 1H). Combined cytoplasmic and nuclear localizations for AGO9  
287 was previously observed by immunolocalization in ovule primordia (Rodríguez-Leal et al.,  
288 2015; Zhao et al., 2018a). However, in those studies, AGO9 was found to accumulate in  
289 cytoplasmic foci which we could not observe with our reporter construct in the tissues  
290 examined. The mCh-AGO8 translational reporter unlike other RddM AGOs, mainly localizes  
291 to the cytoplasm of the egg cell (Fig. 1G). As discussed above, this unusual localization for a  
292 Clade II AGO could be the result of AGO8 being a truncated protein.

293 One of the most intriguing intracellular localization patterns was that of GFP-AGO7. GFP-  
294 AGO7 is mainly localized to the nucleus. However, in some cells of the integument, in the egg  
295 cell and in the central cell, clear cytoplasmic localization is observed, with the presence of  
296 cytoplasmic foci (Fig. 1K-L). Localization of GFP-AGO7 to cytoplasmic foci named “sRNA  
297 bodies” was previously observed in *Nicotiana benthamiana* leaves during transient  
298 overexpression of GFP-AGO7 (Jouannet et al., 2012). Nuclear GFP-AGO7 accumulation was  
299 not reported in this study. The discrepancy could be explained by several factors such as the  
300 difference in the promoter used (*p35S* versus cognate *pAGO7* promoters) and also, importantly,

301 the tissues analyzed (mature leaves or roots *versus* reproductive tissue). Interestingly, retention  
302 of AGO7 in the nucleus using an NLS signal-peptide fused to AGO7 in stable *Arabidopsis*  
303 transformant did not complement the so called leaf zippy phenotype of *ago7* mutant (Hunter  
304 et al., 2003; Jouannet et al., 2012) showing that cytoplasmic localization is necessary for AGO7  
305 function during leaf development. Similarly to AGO7, it was shown that a nuclear retention of  
306 AGO1 do not complement the *ago1* mutant phenotype as AGO1 shuttling between the nucleus  
307 and the cytoplasm is required for its function in the micro RNA pathway (Bologna et al., 2018).  
308 Given that AGO7 zippy mutant phenotype rely on the loading by AGO7 of the micro-RNA  
309 miR390 and that our construct also rescues the of *ago7* mutant *Arabidopsis* (Fig. S6) and  
310 displays both nuclear and cytoplasmic localization in the inspected tissues, it is most likely that  
311 AGO7, similarly to AGO1, shuttles between the nucleus and the cytoplasm and that this  
312 process could be regulated intracellularly during development. Additionally, nuclear AGO7 in  
313 reproductive tissues could have as yet uncharacterized function as shown recently for nuclear  
314 AGO1 (Liu et al., 2018).

315 To conclude, we have generated full locus fluorescently N-term tagged constructs of all  
316 *Arabidopsis* AGOs under their native endogenous promoter. We have analyzed their  
317 expression pattern as well as intracellular localization in reproductive tissues. These constructs  
318 or transgenic lines can be used by the community to study AGOs regulation in a developmental  
319 context as well as during stresses. Fluorescent AGOs reporter were previously reported in  
320 *Arabidopsis* however inconsistencies are present such as the use of overexpression promoters  
321 or C-terminal fusion known to affect the functionality of AGOs protein. We hope these lines  
322 will be beneficial to the community and provide a uniform set of tools for further analysis.

323

## 324 MATERIALS AND METHODS

### 325 PLANT MATERIAL AND GROWTH CONDITIONS

326 After three days at 4°C in the dark, seeds were germinated and grown on soil. Plants were  
327 grown under long days at 20-21°C (16h light/8h night). All plants were in Columbia (Col-0)  
328 accession. The mutants and lines described in this work correspond to the following: *ago1-36*  
329 (SALK\_087076,(Baumberger and Baulcombe, 2005)), *ago2-1* (salk\_003380,(Lobbes et al.,  
330 2006)), *ago3-3* (GABI-743B03,(Jullien et al., 2018)), *ago4-5* (WiscDsLox338A0, (Stroud et  
331 al., 2012)) , *ago5-1* (salk\_063806, (Katiyar-Agarwal et al., 2007)), *ago6-2* (salk\_031553,

332 (Zheng et al., 2007)), *ago7-1* (salk\_037458, (Vazquez et al., 2004)), *ago8-1* (salk\_139894,  
333 (Takeda et al., 2008), *ago9-1* (salk\_127358, (Katiyar-Agarwal et al., 2007)) and *ago10-1*  
334 (SALK\_000457). The insertion lines were provided by The Nottingham *Arabidopsis* Stock  
335 Centre (NASC) (<http://arabidopsis.info/>). Pollen were germinated in Pollen growth medium at  
336 21C in the dark 5 hours to over-night (Hamamura et al., 2011).

#### 337 MICROSCOPY

338 Fluorescence images were acquired using laser scanning confocal microscopy (Zeiss LSM780  
339 or Leica SP5). Brightness was adjusted using ImageJ (<http://rsbweb.nih.gov/ij/>) and assembled  
340 using ImageJ or Adobe Illustrator.

#### 341 PLASMID CONSTRUCTION AND TRANSFORMATION

342 All DNA fragments were amplified by PCR using the Phusion High-Fidelity DNA Polymerase  
343 (Thermo). Primer sequences can be found in Supplementary Table S1. All plasmids were  
344 transformed into their respective mutants and for some also in LIG1-GFP marker line  
345 (Andreuzza et al., 2010). All constructs were generated using Multisite Gateway technology  
346 (Invitrogen). *A. thaliana* transformation was carried out by the floral dip method (Clough and  
347 Bent, 1998). At least six to ten transgenic lines (T1) were analysed and showed a consistent  
348 fluorescence expression pattern using a Leica epifluorescence microscope or a Leica SP5. One  
349 to three independent lines with single insertions, determined by segregation upon BASTA  
350 selection, were used for further detailed confocal analysis.

#### 351 AUTHOR CONTRIBUTIONS

352 PEJ conceived the study. PEJ, NP and JAS generated the transgenic lines. PEJ and DMVB  
353 performed the imaging. DMVB and JAS tested the complementation. PEJ wrote the  
354 manuscript, which was further edited and amended by OV.

#### 355 ACKNOWLEDGEMENTS

356 We would like to thank the following people for their help: Andre Imboden and Jasmine  
357 Sekulovski for support in plant growth, Nicolas G. Bologna for critical reading of the  
358 manuscript We would like to thank the ETH Scope M and Microscopy Imaging Center of the  
359 University of Bern.

#### 360 FUNDING

361 This project was supported by a core grant from ETH-Z attributed to OV. PEJ (Project 329404)  
362 and NP (Project 299789) were supported by Marie Curie fellowships hosted in OV's laboratory

363 at ETH-Z. PEJ, DMVB and JAS are supported by an SNF professorship grant (no.163946)  
364 attributed to PEJ.

365 *COMPETING INTERESTS*

366 The authors have no conflicts of interest to declare.

367 *SUPPLEMENTARY INFORMATION*

368 Additional Supporting Information may be found in the online version of this article

369 REFERENCES

- 370 **Andreuzza, S., Li, J., Guitton, A.-E., Faure, J.-E., Casanova, S., Park, J.-S., Choi, Y.,**  
371 **Chen, Z. and Berger, F.** (2010). DNA LIGASE I exerts a maternal effect on seed  
372 development in *Arabidopsis thaliana*. *Development* **137**, 73–81.
- 373 **Baumberger, N. and Baulcombe, D. C.** (2005). *Arabidopsis* ARGONAUTE1 is an RNA  
374 Slicer that selectively recruits microRNAs and short interfering RNAs. *Proc. Natl. Acad.*  
375 *Sci. U. S. A.* **102**, 11928–11933.
- 376 **Belmonte, M. F., Kirkbride, R. C., Stone, S. L., Pelletier, J. M., Bui, A. Q., Yeung, E. C.,**  
377 **Hashimoto, M., Fei, J., Harada, C. M., Munoz, M. D., et al.** (2013). Comprehensive  
378 developmental profiles of gene activity in regions and subregions of the *Arabidopsis*  
379 seed. *Proc. Natl. Acad. Sci.* **110**, E435–E444.
- 380 **Bologna, N. G., Iselin, R., Abriata, L. A., Sarazin, A., Pumplun, N., Jay, F., Grentzinger,**  
381 **T., Dal Peraro, M. and Voinnet, O.** (2018). Nucleo-cytosolic Shuttling of  
382 ARGONAUTE1 Prompts a Revised Model of the Plant MicroRNA Pathway. *Mol. Cell*  
383 **69**, 709-719.e5.
- 384 **Borges, F., Pereira, P. a, Slotkin, R. K., Martienssen, R. a and Becker, J. D.** (2011).  
385 MicroRNA activity in the *Arabidopsis* male germline. *J. Exp. Bot.* **62**, 1611–20.
- 386 **Borges, F., Parent, J. S., Van Ex, F., Wolff, P., Martínez, G., Köhler, C. and**  
387 **Martienssen, R. A.** (2018). Transposon-derived small RNAs triggered by miR845  
388 mediate genome dosage response in *Arabidopsis*. *Nat. Genet.* **50**, 186–192.
- 389 **Bouyer, D., Kramdi, A., Kassam, M., Heese, M., Schnittger, A., Roudier, F. and Colot,**  
390 **V.** (2017). DNA methylation dynamics during early plant life. *Genome Biol.* **18**, 179.
- 391 **Carbonell, A., Fahlgren, N., Garcia-Ruiz, H., Gilbert, K. B., Montgomery, T. a, Nguyen,**  
392 **T., Cuperus, J. T. and Carrington, J. C.** (2012). Functional analysis of three  
393 *Arabidopsis* ARGONAUTES using slicer-defective mutants. *Plant Cell* **24**, 3613–29.
- 394 **Castel, S. E. and Martienssen, R. A.** (2013). RNA interference in the nucleus: Roles for  
395 small RNAs in transcription, epigenetics and beyond. *Nat. Rev. Genet.* **14**, 100–112.
- 396 **Clough, S. J. and Bent, A. F.** (1998). Floral dip: A simplified method for *Agrobacterium*-

- 397 mediated transformation of *Arabidopsis thaliana*. *Plant J.* **16**, 735–743.
- 398 **Conine, C. C., Sun, F., Song, L., Rivera-Pérez, J. A. and Rando, O. J.** (2018). Small  
399 RNAs Gained during Epididymal Transit of Sperm Are Essential for Embryonic  
400 Development in Mice. *Dev. Cell* **46**, 470-480.e3.
- 401 **Cranfill, P. J., Sell, B. R., Baird, M. A., Allen, J. R., Lavagnino, Z., De Gruiter, H. M.,**  
402 **Kremers, G. J., Davidson, M. W., Ustione, A. and Piston, D. W.** (2016). Quantitative  
403 assessment of fluorescent proteins. *Nat. Methods* **13**, 557–562.
- 404 **Du, F., Gong, W., Boscá, S., Tucker, M., Vaucheret, H. and Laux, T.** (2019). Dose-  
405 Dependent AGO1-Mediated Inhibition of the miRNA165/166 Pathway Modulates Stem  
406 Cell Maintenance in Arabidopsis Shoot Apical Meristem. *Plant Commun.* 100002.
- 407 **Ebhardt, H. A., Fedynak, A. and Fahlman, R. P.** (2010). Naturally occurring variations in  
408 sequence length creates microRNA isoforms that differ in argonaute effector complex  
409 specificity. *Silence* **1**, 1–6.
- 410 **Fang, X. and Qi, Y.** (2015). Rnai in plants: An argonaute-centered view. *Plant Cell* **28**, 272–  
411 285.
- 412 **Gehring, M., Bubb, K. L. and Henikoff, S.** (2009). Extensive demethylation of repetitive  
413 elements during seed development underlies gene imprinting. *Science (80-. ).* **324**,  
414 1447–51.
- 415 **Gutzat, R., Rembart, K., Nussbaumer, T., Pisupati, R., Hofmann, F., Bradamante, G.,**  
416 **Daubel, N., Gaidora, A., Lettner, N., Donà, M., et al.** (2018). Stage-specific  
417 transcriptomes and DNA methylomes indicate an early and transient loss of transposon  
418 control in Arabidopsis shoot stem cells. *bioRxiv*.
- 419 **Hamamura, Y., Saito, C., Awai, C., Kurihara, D., Miyawaki, A., Nakagawa, T.,**  
420 **Kanaoka, M. M., Sasaki, N., Nakano, A., Berger, F., et al.** (2011). Live-cell imaging  
421 reveals the dynamics of two sperm cells during double fertilization in Arabidopsis  
422 *thaliana*. *Curr. Biol.* **21**, 497–502.
- 423 **Havecker, E. R., Wallbridge, L. M., Hardcastle, T. J., Bush, M. S., Kelly, K. A., Dunn,**  
424 **R. M., Schwach, F., Doonan, J. H. and Baulcombe, D. C.** (2010). The Arabidopsis  
425 RNA-directed DNA methylation argonautes functionally diverge based on their

- 426 expression and interaction with target loci. *Plant Cell* **22**, 321–34.
- 427 **He, J., Xu, M., Willmann, M. R., McCormick, K., Hu, T., Yang, L., Starker, C. G.,**  
428 **Voytas, D. F., Meyers, B. C. and Poethig, R. S.** (2018). Threshold-dependent  
429 repression of SPL gene expression by miR156/miR157 controls vegetative phase change  
430 in *Arabidopsis thaliana*. *PLoS Genet.* **14**, 1–28.
- 431 **Hernández-Lagana, E., Rodríguez-Leal, D., Lúa, J. and Vielle-Calzada, J. P.** (2016). A  
432 multigenic network of ARGONAUTE4 clade members controls early megaspore  
433 formation in *Arabidopsis*. *Genetics* **204**, 1045–1056.
- 434 **Hsieh, T. T.-F., Ibarra, C. A., Silva, P., Zemach, A., Eshed-Williams, L., Fischer, R. L.**  
435 **and Zilberman, D.** (2009). Genome-wide demethylation of *Arabidopsis* endosperm.  
436 *Science (80-. ).* **324**, 1451–1454.
- 437 **Hunter, C., Sun, H. and Poethig, R. S.** (2003). The *Arabidopsis* Heterochronic Gene ZIPPY  
438 Is an ARGONAUTE Family Member. *Curr. Biol.* **13**, 1734–1739.
- 439 **Jouannet, V., Moreno, A. B., Elmayan, T., Vaucheret, H., Crespi, M. D. and Maizel, A.**  
440 (2012). Cytoplasmic *Arabidopsis* AGO7 accumulates in membrane-associated siRNA  
441 bodies and is required for ta-siRNA biogenesis. *EMBO J.* **31**, 1704–1713.
- 442 **Jullien, P. E. P. E., Susaki, D., Yelagandula, R., Higashiyama, T. and Berger, F.** (2012).  
443 DNA methylation dynamics during sexual reproduction in *Arabidopsis thaliana*. *Curr.*  
444 *Biol.* **22**, in press.
- 445 **Jullien, P. E., Grob, S., Marchais, A., Pumplin, N., Chevalier, C., Otto, C., Schott, G.**  
446 **and Voinnet, O.** (2018). Functional characterization of *Arabidopsis* ARGONAUTE 3 in  
447 reproductive tissue. *bioRxiv* 500769.
- 448 **Katiyar-Agarwal, S., Gao, S., Vivian-Smith, A. and Jin, H.** (2007). A novel class of  
449 bacteria-induced small RNAs in *Arabidopsis*. *Genes Dev.* **21**, 3123–3134.
- 450 **Kawakatsu, T., Nery, J. R., Castanon, R. and Ecker, J. R.** (2017). Dynamic DNA  
451 methylation reconfiguration during seed development and germination. *Genome Biol.*  
452 **18**, 171.
- 453 **Landgraf, D., Okumus, B., Chien, P., Baker, T. A. and Paulsson, J.** (2012). Segregation  
454 of molecules at cell division reveals native protein localization. *Nat. Methods* **9**, 480–



- 455 482.
- 456 **Liu, C., Xin, Y., Xu, L., Cai, Z., Xue, Y., Liu, Y., Xie, D., Liu, Y. and Qi, Y.** (2018).  
457 *Arabidopsis ARGONAUTE 1 Binds Chromatin to Promote Gene Transcription in*  
458 *Response to Hormones and Stresses. Dev. Cell* **44**, 348-361.e7.
- 459 **Lobbes, D., Rallapalli, G., Schmidt, D. D., Martin, C. and Clarke, J.** (2006). *SERRATE:*  
460 *a new player on the plant microRNA scene. EMBO Rep.* **7**, 1052–8.
- 461 **Lynn, K., Fernandez, A., Aida, M., Sedbrook, J., Tasaka, M., Masson, P. and Barton,**  
462 **M. K.** (1999). The PINHEAD/ZWILLE gene acts pleiotropically in Arabidopsis  
463 development and has overlapping functions with the ARGONAUTE1 gene.  
464 *Development* **126**, 469–481.
- 465 **Mallory, A. and Vaucheret, H.** (2010). Form, function, and regulation of ARGONAUTE  
466 proteins. *Plant Cell* **22**, 3879–89.
- 467 **Martinez, G., Wolff, P., Wang, Z., Moreno-Romero, J., Santos-González, J., Conze, L.**  
468 **L., Defraia, C., Slotkin, R. K. and Köhler, C.** (2018). Paternal easiRNAs regulate  
469 parental genome dosage in Arabidopsis. *Nat. Genet.* **50**, 193–198.
- 470 **Matzke, M. A. and Mosher, R. A.** (2014). RNA-directed DNA methylation: An epigenetic  
471 pathway of increasing complexity. *Nat. Rev. Genet.* **15**, 394–408.
- 472 **Meinke, D. W.** (2020). Genome-wide identification of EMBRYO-DEFECTIVE (EMB)  
473 genes required for growth and development in Arabidopsis. *New Phytol.* **226**, 306–325.
- 474 **Mosher, R. A. and Melnyk, C. W.** (2010). siRNAs and DNA methylation: seedy  
475 epigenetics. *Trends Plant Sci.* **15**, 204–210.
- 476 **Moussian, B., Schoof, H., Haecker, A., Ju, G. and Laux, T.** (1998). Role of the ZWILLE  
477 gene in the regulation of central shoot meristem cell fate during Arabidopsis  
478 embryogenesis. *Curr. Opin. Plant Biol.* **1**, 188.
- 479 **Nodine, M. D. and Bartel, D. P.** (2010). MicroRNAs prevent precocious gene expression  
480 and enable pattern formation during plant embryogenesis. *Genes Dev.* **24**, 2678–92.
- 481 **Oliver, C., Santos, J. L. and Pradillo, M.** (2014). On the role of some ARGONAUTE  
482 proteins in meiosis and DNA repair in Arabidopsis thaliana. *Front. Plant Sci.* **5**, 177.

- 483 **Olmedo-Monfil, V., Durán-Figueroa, N., Arteaga-Vázquez, M., Demesa-Arévalo, E.,**  
484 **Autran, D., Grimanelli, D., Slotkin, R. K., Martienssen, R. A. and Vielle-Calzada,**  
485 **J.-P.** (2010). Control of female gamete formation by a small RNA pathway in  
486 Arabidopsis. *Nature* **464**, 628–632.
- 487 **Rodríguez-Leal, D., León-Martínez, G., Abad-Vivero, U. and Vielle-Calzada, J. P.**  
488 (2015). Natural variation in epigenetic pathways affects the specification of female  
489 gamete precursors in arabidopsis. *Plant Cell* **27**, 1034–1045.
- 490 **Roussin-Léveillé, C., Silva-Martins, G. and Moffett, P.** (2020). ARGONAUTE5  
491 Represses Age-Dependent Induction of Flowering through Physical and Functional  
492 Interaction with miR156 in Arabidopsis. *Plant Cell Physiol.* **61**, 957–966.
- 493 **Seefried, W. F., Willmann, M. R., Clausen, R. L. and Jenik, P. D.** (2014). Global  
494 regulation of embryonic patterning in arabidopsis by MicroRNAs. *Plant Physiol.* **165**,  
495 670–687.
- 496 **Sharma, U., Sun, F., Conine, C. C., Reichholf, B., Kukreja, S., Herzog, V. A., Ameres, S.**  
497 **L. and Rando, O. J.** (2018). Small RNAs Are Trafficked from the Epididymis to  
498 Developing Mammalian Sperm. *Dev. Cell* **46**, 481-494.e6.
- 499 **Slotkin, R. K., Vaughn, M., Borges, F., Tanurdzic, M., Becker, J. D. J. D., Feijo, J. A.,**  
500 **Martienssen, R. A., Tanurdžić, M., Feijó, J. A., Feijo, A., et al.** (2009). Epigenetic  
501 reprogramming and small RNA silencing of transposable elements in pollen. *Cell* **136**,  
502 461–472.
- 503 **Sprunck, S., Urban, M., Strieder, N., Lindemeier, M., Bleckmann, A., Evers, M.,**  
504 **Hackenberg, T., Möhle, C., Dresselhaus, T. and Engelmann, J. C.** (2019).  
505 Elucidating small RNA pathways in Arabidopsis thaliana egg cells. *bioRxiv*.
- 506 **Stroud, H., Greenberg, M. V. C., Feng, S., Bernatavichute, Y. V. and Jacobsen, S. E.**  
507 (2012). Resource Comprehensive Analysis of Silencing Mutants Reveals Complex  
508 Regulation of the Arabidopsis Methylome. *Cell* **152**, 352–364.
- 509 **Takeda, A., Iwasaki, S., Watanabe, T., Utsumi, M. and Watanabe, Y.** (2008). The  
510 mechanism selecting the guide strand from small RNA duplexes is different among  
511 Argonaute proteins. *Plant Cell Physiol.* **49**, 493–500.

- 512 **Tucker, M. R., Hinze, A., Tucker, E. J., Takada, S., Jürgens, G. and Laux, T.** (2008).  
513 Vascular signalling mediated by ZWILLE potentiates WUSCHEL function during shoot  
514 meristem stem cell development in the Arabidopsis embryo. *Development* **135**, 2839–  
515 2843.
- 516 **Tucker, M. R., Okada, T., Hu, Y., Scholefield, A., Taylor, J. M. and Koltunow, A. M. G.**  
517 (2012). Somatic small RNA pathways promote the mitotic events of megagametogenesis  
518 during female reproductive development in Arabidopsis. *Development* **139**, 1399–1404.
- 519 **Van Ex, F., Jacob, Y. and Martienssen, R. a** (2011). Multiple roles for small RNAs during  
520 plant reproduction. *Curr. Opin. Plant Biol.* 1–6.
- 521 **Vazquez, F., Gascioli, V., Crété, P. and Vaucheret, H.** (2004). The Nuclear dsRNA  
522 Binding Protein HYL1 Is Required for MicroRNA Accumulation and Plant  
523 Development, but Not Posttranscriptional Transgene Silencing. *Curr. Biol.* **14**, 346–351.
- 524 **Weick, E. M. and Miska, E. A.** (2014). piRNAs: From biogenesis to function. *Dev.* **141**,  
525 3458–3471.
- 526 **Willmann, M. R., Mehalick, A. J., Packer, R. L. and Jenik, P. D.** (2011). MicroRNAs  
527 regulate the timing of embryo maturation in Arabidopsis. *Plant Physiol.* **155**, 1871–  
528 1884.
- 529 **Wu, G., Park, M. Y., Conway, S. R., Wang, J. W., Weigel, D. and Poethig, R. S.** (2009).  
530 The Sequential Action of miR156 and miR172 Regulates Developmental Timing in  
531 Arabidopsis. *Cell* **138**, 750–759.
- 532 **Wuest, S. E., Vijverberg, K., Schmidt, A., Weiss, M., Gheyselinck, J., Lohr, M.,**  
533 **Wellmer, F., Rahnenführer, J., von Mering, C. and Grossniklaus, U.** (2010).  
534 Arabidopsis Female Gametophyte Gene Expression Map Reveals Similarities between  
535 Plant and Animal Gametes. *Curr. Biol.* **20**, 506–512.
- 536 **Ye, R., Wang, W., Iki, T., Liu, C., Wu, Y., Ishikawa, M., Zhou, X. and Qi, Y.** (2012).  
537 Cytoplasmic Assembly and Selective Nuclear Import of Arabidopsis  
538 ARGONAUTE4/siRNA Complexes. *Mol. Cell* **46**, 859–870.
- 539 **Yuan, S., Schuster, A., Tang, C., Yu, T., Ortogero, N., Bao, J., Zheng, H. and Yan, W.**  
540 (2016). Sperm-borne miRNAs and endo-siRNAs are important for fertilization and

- 541 preimplantation embryonic development. *Dev.* **143**, 635–647.
- 542 **Zhang, H., Xia, R., Meyers, B. C. and Walbot, V.** (2015). Evolution, functions, and  
543 mysteries of plant ARGONAUTE proteins. *Curr. Opin. Plant Biol.* **27**, 84–90.
- 544 **Zhao, L., Cai, H., Su, Z., Wang, L., Huang, X., Zhang, M., Chen, P., Dai, X., Zhao, H.,**  
545 **Palanivelu, R., et al.** (2018a). KLU suppresses megasporocyte cell fate through SWR1-  
546 mediated activation of WRKY28 expression in Arabidopsis. *Proc. Natl. Acad. Sci. U. S.*  
547 *A.* **115**, E526–E535.
- 548 **Zhao, Y., Wang, S., Wu, W., Li, L., Jiang, T. and Zheng, B.** (2018b). Clearance of  
549 maternal barriers by paternal miR159 to initiate endosperm nuclear division in  
550 Arabidopsis. *Nat. Commun.* **9**, 5011.
- 551 **Zheng, X., Zhu, J., Kapoor, A. and Zhu, J.-K.** (2007). Role of Arabidopsis AGO6 in  
552 siRNA accumulation, DNA methylation and transcriptional gene silencing. *EMBO J.* **26**,  
553 1691–1701.
- 554
- 555

556 FIGURE LEGENDS

557

558 **Fig. 1.** AGOs accumulation in the mature female gametophyte. (A) schematic representation  
559 of a mature female gametophyte of *Arabidopsis thaliana* illustrating the three major cell types:  
560 the central cell (cc) in green, the egg cell (ec) in orange, the synergides (syn) in blue. The  
561 mature female gametophyte is surrounded by maternal sporophytic tissue represented in grey,  
562 including the inner integument (ii), outer integument (oi) and the nucellus (nuc). (B-K)  
563 Confocal images representing the expression of the 10 *Arabidopsis* AGOs in mature female  
564 gametophytes: mCherry-AGO1 (B), mCherry-AGO5 (C), GFP-AGO10 (D), mCherry-AGO4  
565 (E), mCherry-AGO6 (F), mCherry-AGO8 (G), mCherry-AGO9 (H), mCherry-AGO2 (I),  
566 mCherry-AGO3 (J) and GFP-AGO7 (K). (L) Confocal image of the intra-cellular localization  
567 of GFP-AGO7 in the egg cell and central cell. Scale bars represent 10µm.

568

569 **Fig. 2.** AGOs accumulation in the pollen. (A-H) AGOs in the mature male gametophyte. (A)  
570 Schematic representation of a mature pollen grain of *Arabidopsis thaliana* illustrating the two  
571 major cell types: the vegetative cell (v) and the two sperm cells (s). (B-H) Confocal images  
572 representing the expression of seven *Arabidopsis* AGOs accumulating in the pollen grain:  
573 mCherry-AGO1 (B), mCherry-AGO5 (C), mCherry-AGO4 (D), mCherry-AGO6 (E),  
574 mCherry-AGO9 (F), mCherry-AGO2 (G) and GFP-AGO7 (H). (I-P) AGO accumulation in  
575 germinating pollen tube. (I) Schematic representation of a growing pollen tube of *Arabidopsis*  
576 *thaliana* illustrating the two sperm cells (s). (J-P) Confocal images of the seven *Arabidopsis*  
577 AGOs in germinated pollen grain: mCherry-AGO1 (B), mCherry-AGO5 (C), mCherry-AGO4  
578 (D), mCherry-AGO6 (E), mCherry-AGO9 (F), mCherry-AGO2 (G) and GFP-AGO7 (H).  
579 Scale bars represent 5 µm.

580

581 **Fig. 3.** AGOs accumulation in the developing seed. (A-I) Confocal images of the height  
582 *Arabidopsis* AGOs expressed in the developing seeds 2 days-after-pollination (DAP):  
583 mCherry-AGO1 (A), mCherry-AGO5 (B), GFP-AGO10 (C), mCherry-AGO4 (D-E),  
584 mCherry-AGO6 (F), mCherry-AGO9 (G), mCherry-AGO3 (H) and GFP-AGO7 (I). Scale bars  
585 represent 10 µm. Abbreviation: emb (embryo), endo (endosperm), inner integument (ii), outer  
586 integuments (oi), Chalazal seed coat (czsc).

587 **Fig. 4.** AGOs accumulation in the heart-stage embryo. (A) A simplified representation of a  
588 heart-stage embryo of *Arabidopsis thaliana* illustrating the different cell types. (B-H) Confocal  
589 images of the seven Arabidopsis AGOs accumulating in the heart-stage embryo: mCherry-  
590 AGO1 (B), mCherry-AGO5 (C), GFP-AGO10 (D), mCherry-AGO4 (E), mCherry-AGO6 (F),  
591 mCherry-AGO9 (G), and GFP-AGO7 (H). Scale bars represent 10  $\mu$ m.

592

593 **Fig. S1.** Schematic representation of the constructs used in this study. The different features  
594 are represented by arrows: promoter (purple), UTRs (yellow), fluorescent protein (red), exon  
595 (green) and additional annotations (blue).

596

597 **Fig. S2.** Complementation of the *ago1-36* mutant *Arabidopsis* by *pAGO1:mCherry-AGO1*.  
598 Representative pictures showing the rescue of the string developmental phenotype in Col-0 (A)  
599 and mCh1 #9 *ago1-36*-(C) compared to *ago1-36*-. scale bar represents 1mm.

600

601 **Fig. S3.** Complementation of *ago4-5* mutant by *pAGO4:mCherry-AGO4*. qPCR showing the  
602 absence of *AtSN1* ectopic expression in rosette leaves of seven independent lines expressing  
603 the construct *pAGO4:mCherry-AGO4* (*mCh4*) in *ago4-5* background compared to Col-0 and  
604 *ago4-5*. Actin2 was used as endogenous control. p indicates the p value obtained by a Student's  
605 T-Test.

606

607 **Fig. S4.** Complementation of *ago5-1* mutant *Arabidopsis* by *pAGO5:mCherry-AGO5*. (A)  
608 Representative pictures of the early flowering phenotype of *ago5-1*- compared to Col-0 and  
609 mCh5 #29 *ago5-1*-. (B) Quantification of *ago5-1*- flowering phenotype in *ago5-1*- (n=27),  
610 Col-0 (n=26) and mCh5#29 *ago5-1*- (n=27).

611

612 **Fig. S5.** Complementation of *ago6-2* mutant by *pAGO6:mCherry-AGO6*. qPCR showing the  
613 absence of *AtSN1* ectopic expression in rosette leaves of seven independent lines expressing  
614 the construct *pAGO6:mCherry-AGO6* (*mCh4*) in *ago6-2* background compared to Col-0 and

615 *ago6-2*. Actin2 was used as endogenous control. p indicates the p value obtained by a Student's  
616 T-Test.

617

618 **Fig. S6.** Complementation of *ago7-1* mutant *Arabidopsis* by *pAGO7:GFP-AGO7*. Illustrative  
619 pictures of the leaf “zippy” phenotype of *ago7-1/-* (B) compared to Col-0 (A) and GFP-AGO7  
620 *ago7-1/-* (C). n= 7

621

622 **Fig. S7.** Additional pictures of *pAGO10:GFP-AGO10*. (A-B) Picture of the accumulation in  
623 ovules of GFP-AGO10 in the vascular tissue of the funiculus (funi) and at the vascular  
624 termination of the chalazal seed coat (czsc). Scale bars represent 10  $\mu$ m.

625

626 **Fig. S8.** Additional pictures of *pAGO9:mCh-AGO9*. (A) Pictures of the expression in ovules  
627 of mCherry-AGO9 in the funiculus (funi) and in the chalazal seed coat (czsc). (B-C)  
628 Accumulation of mCherry-AGO9 in developing seeds, in early embryo and endosperm, 17  
629 hours after pollination (HAP) (B) or 24 HAP (C). Scale bars represent 10  $\mu$ m.

630

631 **Fig. S9.** *Arabidopsis* AGO transcription patterns extracted from microarray data of LCM-  
632 dissected female gametophytes (Wuest et al, 2010) confirming the general enrichment of AGO  
633 transcripts in the egg cell (EC) compared to central cell (CC) or synergids (Syn). (A) Violin  
634 plot representing the general enrichment of AGO transcripts in the EC. (B) AGOs individual  
635 expression boxplot in the different cell types. p values of a Wilcoxon test are indicated.

636

637 **Fig. S10.** *Arabidopsis* AGO transcription patterns extracted from microarray data of LCM-  
638 dissected seeds at the pre-globular stage (Belmonte et al., 2013) confirming the general  
639 enrichment of AGO transcripts in the embryo compared to the peripheral endosperm. (A)  
640 Violin plot representing the general enrichment of AGO transcripts in the embryo. (B) AGOs  
641 individual expression boxplot in the different cell types. p values of a Wilcoxon test are  
642 indicated. *AGO6* and *AGO8* probes are not present in these data.

643

644 **Fig S11.** Summary table of AGO's expression pattern in reproductive tissues.

645



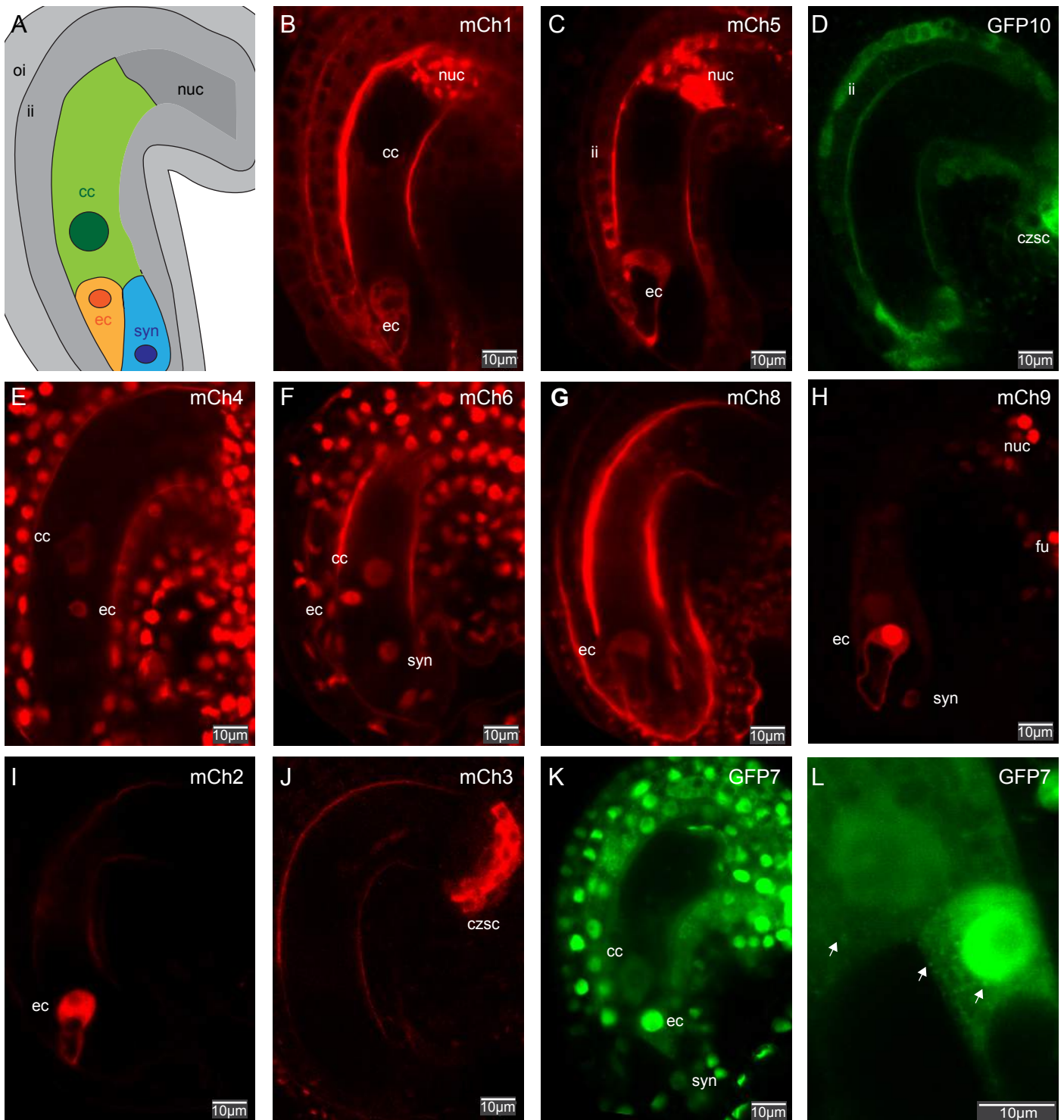


Fig. 1. Argonaute expression in the mature female gametophyte. (A) schematic representation of a mature female gametophyte of *Arabidopsis thaliana* illustrating the three major cell type: the central cell (cc) in green, the egg cell (ec) in orange, the synergides (syn) in blue. The mature female gametophyte is surrounded by maternal sporophytic tissue represented in grey including the inner integument (ii), outer integument (oi) and the nucellus (nuc). (B-K) Confocal images representing the expression of the 10 Arabidopsis AGOs in mature female gametophyte: mCherry-AGO1 (B), mCherry-AGO5 (C), GFP-AGO10 (D), mCherry-AGO4 (E), mCherry-AGO6 (F), mCherry-AGO8 (G), mCherry-AGO9 (H), mCherry-AGO2 (I), mCherry-AGO3 (J) and GFP-AGO7 (K). (L) Confocal image illustrating the intra-cellular localization of GFP-AGO7 in the egg cell and central cell. Scale bars represent 10µm.

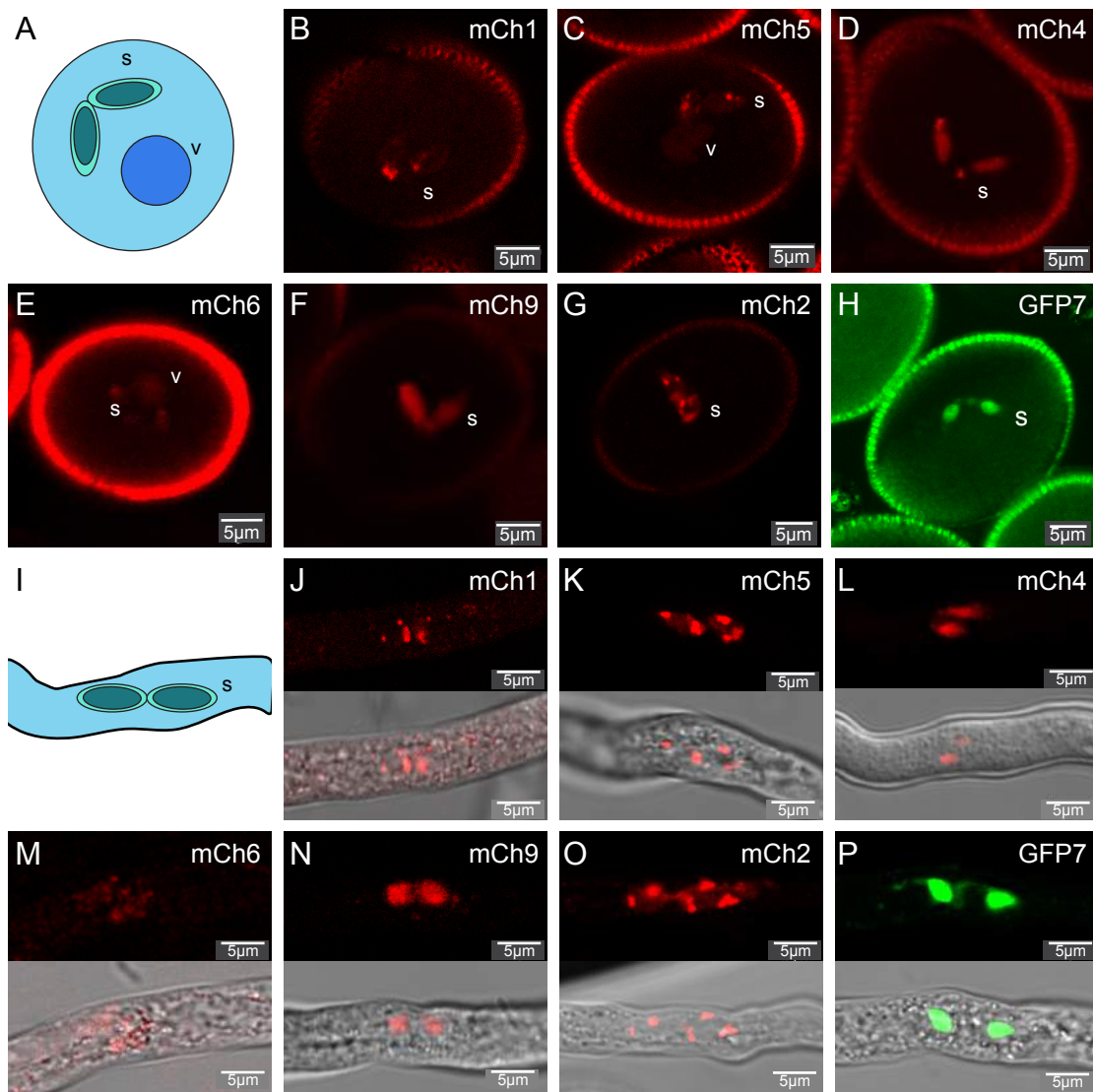


Fig. 2. Argonaute expression in pollen. (A-H) AGOs in the mature male gametophyte. (A) Schematic representation of a mature pollen grain of *Arabidopsis thaliana* illustrating the two major cell type: the vegetative cell (v) and the two sperm cells (s). (B-H) Confocal images representing the expression of 7 *Arabidopsis* AGOs expressed in the pollen grain: mCherry-AGO1 (B), mCherry-AGO5 (C), mCherry-AGO4 (D), mCherry-AGO6 (E), mCherry-AGO9 (F), mCherry-AGO2 (G) and GFP-AGO7 (H). (I-P) Argonaute expression in germinating pollen tube. (I) Schematic representation of a growing pollen tube of *Arabidopsis thaliana* illustrating the two sperm cells (s). (J-P) Confocal images representing the 7 *Arabidopsis* AGOs expressed in in germinated pollen grain: mCherry-AGO1 (B), mCherry-AGO5 (C), mCherry-AGO4 (D), mCherry-AGO6 (E), mCherry-AGO9 (F), mCherry-AGO2 (G) and GFP-AGO7 (H). Scale bars represent 5 µm.

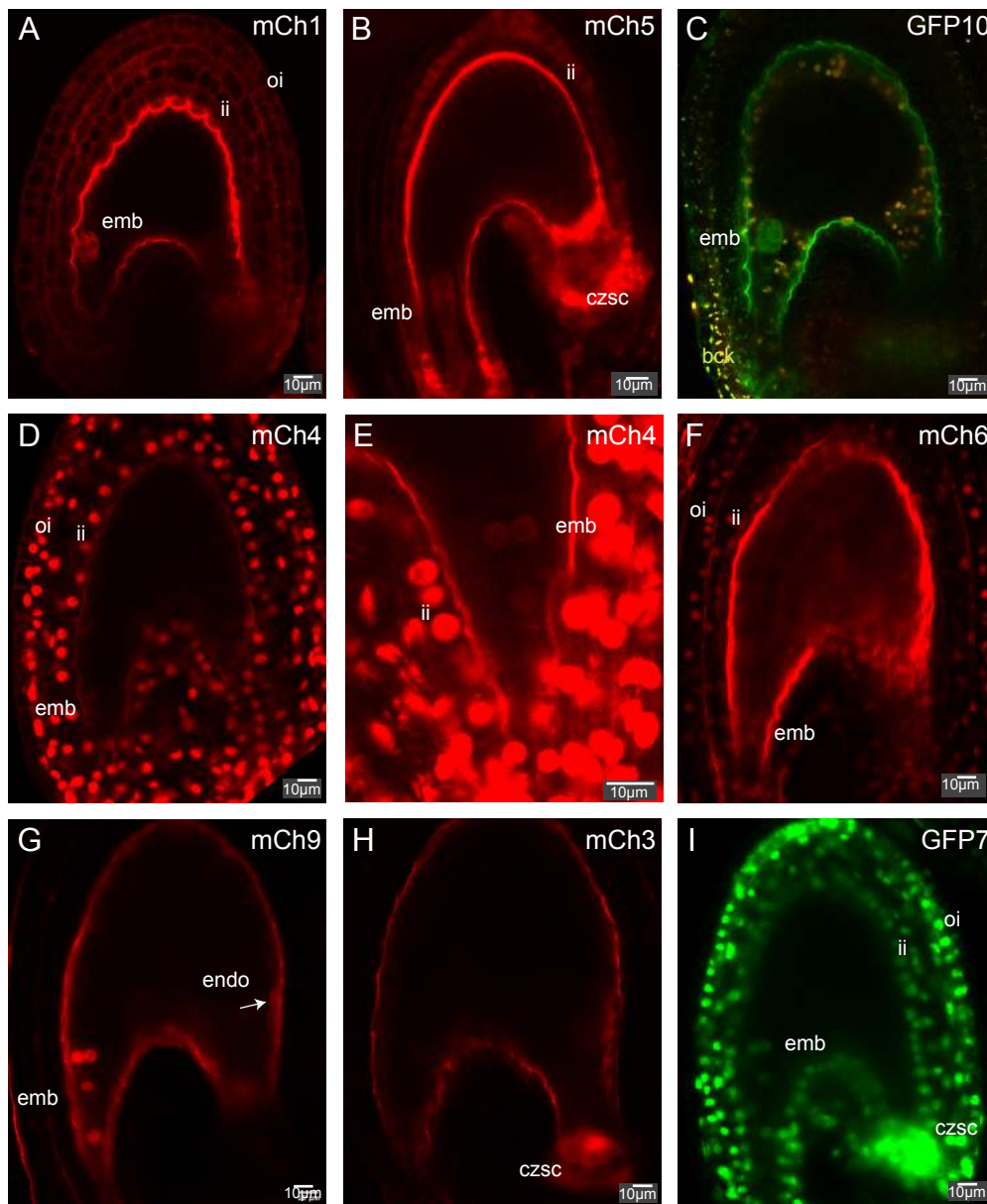


Fig. 3. Argonaute expression in developing seed. (A-I) Confocal images representing Arabidopsis AGOs expressed in the developing seeds at 2 day after pollination: mCherry-AGO1 (A), mCherry-AGO5 (B), GFP-AGO10 (C), mCherry-AGO4 (D-E), mCherry-AGO6 (F), mCherry-AGO9 (G), mCherry-AGO3 (H) and GFP-AGO7 (I). Scale bars represent 10  $\mu$ m. Abbreviation: emb (embryo), endo (endosperm), inner integument (ii), outer integuments (oi), Chalazal seed coat (czsc).

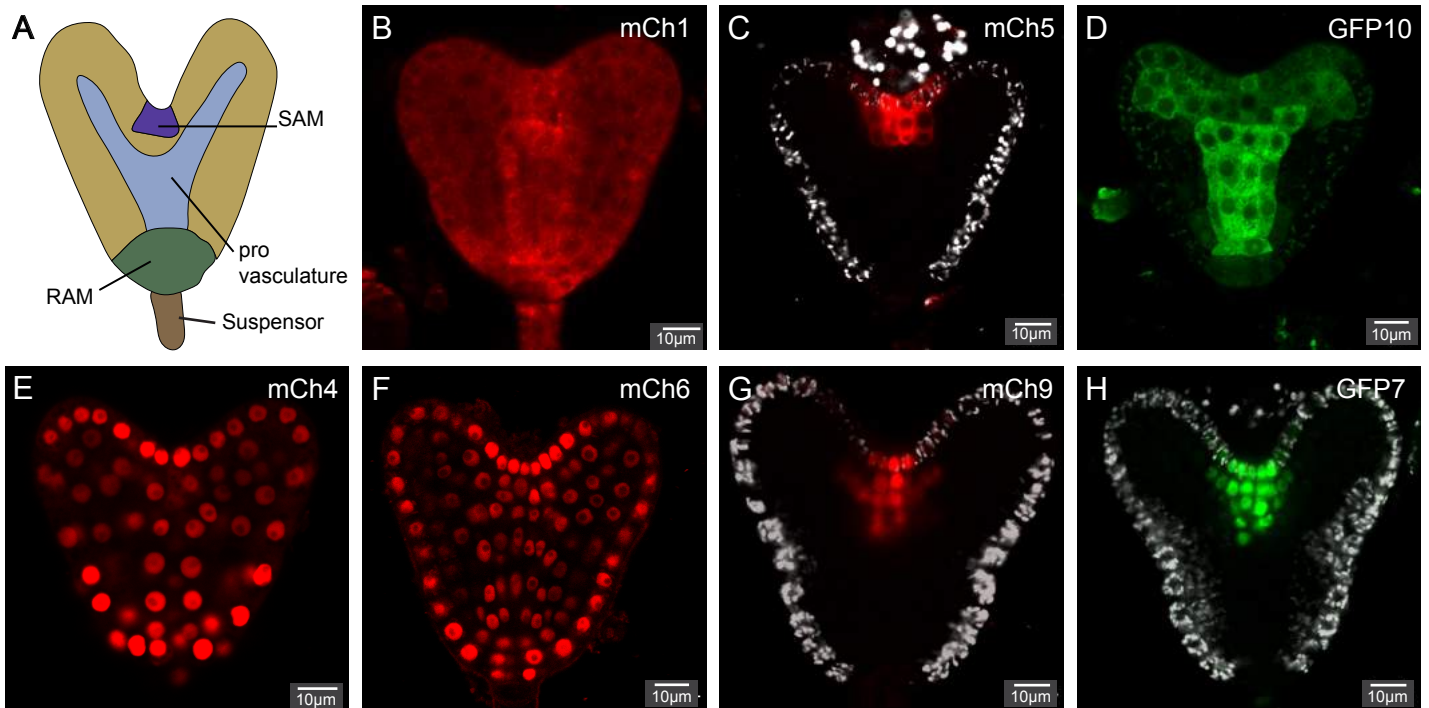


Fig. 4. Argonaute expression in heart stage embryo. (A) A simplified representation of a heart stage embryo illustrating the different cell types. (B-H) Confocal images representing the 7 Arabidopsis AGOs expressed in heart stage embryo: mCherry-AGO1 (B), mCherry-AGO5 (C), GFP-AGO10 (D), mCherry-AGO4 (E), mCherry-AGO6 (F), mCherry-AGO9 (G), and GFP-AGO7 (H). Scale bars represent 10 µm.

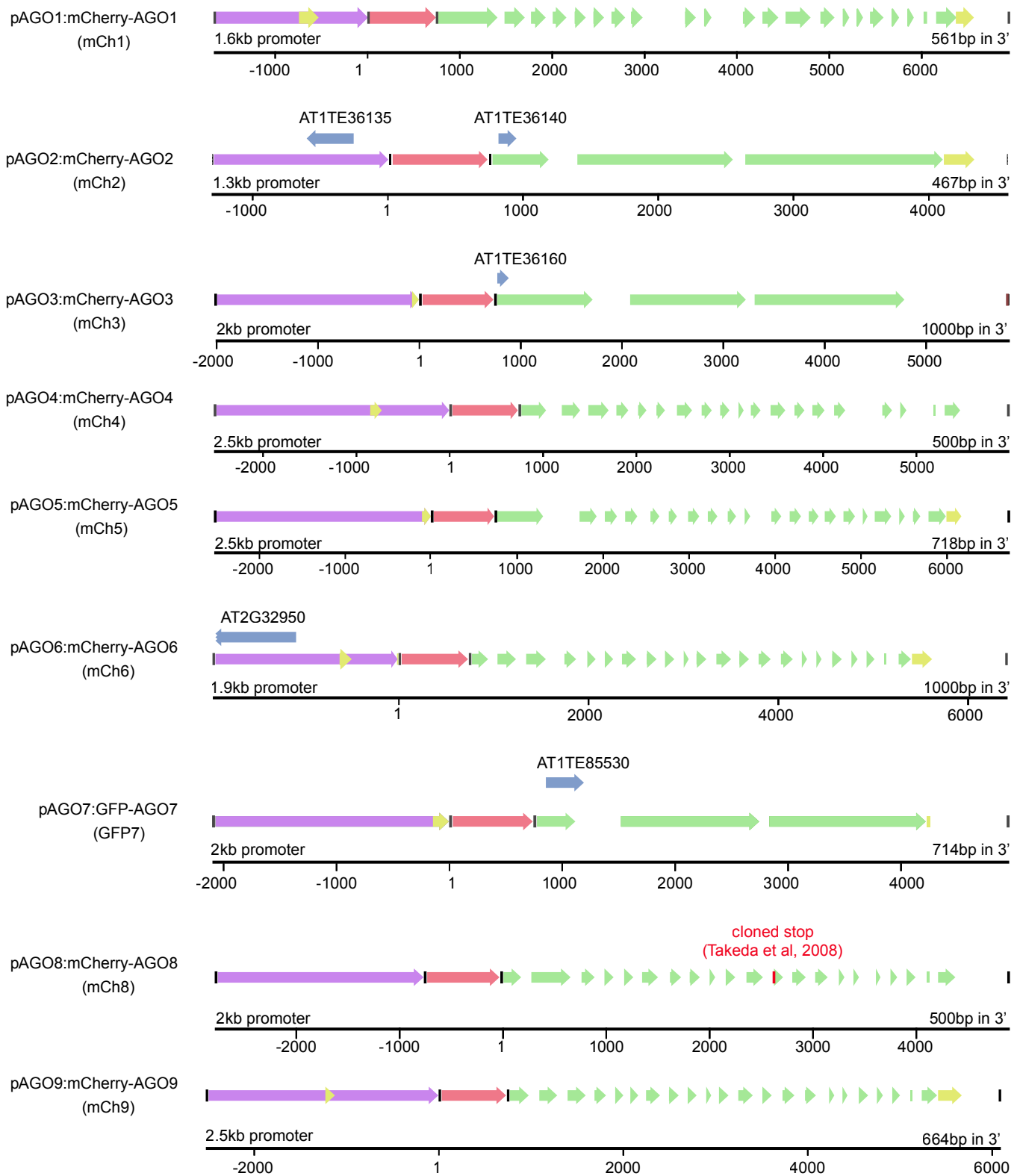


Fig. S1. Schematic representation of the construct used in this study. The different features are represented by arrows: promoter (purple), UTR (yellow), fluorescent protein (red), exon (green) and additional annotation (blue).



Fig. S2. Complementation of *ago1-36* mutant by pAGO1:mCherry-AGO1. Illustrative pictures showing the lack of developmental phenotype in Col-0 (A) and *mCh1 #9 ago1-36/-* (C) compared to *ago1-36/-*. scale bar represents 1mm.

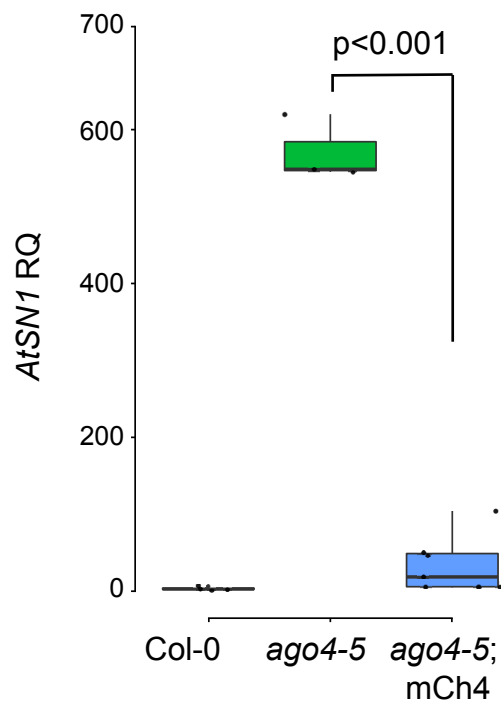


Fig. S3. Complementation of ago4-5 mutant by pAGO4:mCherry-AGO4. qPCR showing the absence of AtSN1 ectopic expression in rosette leaves of seven independent lines expressing the construct pAGO4:mCherry-AGO4 (mCh4) in ago4-5 background compared to Col-0 and ago4-5. Actin2 was used as endogenous control. p indicates the p value obtained by a Student's T-Test.

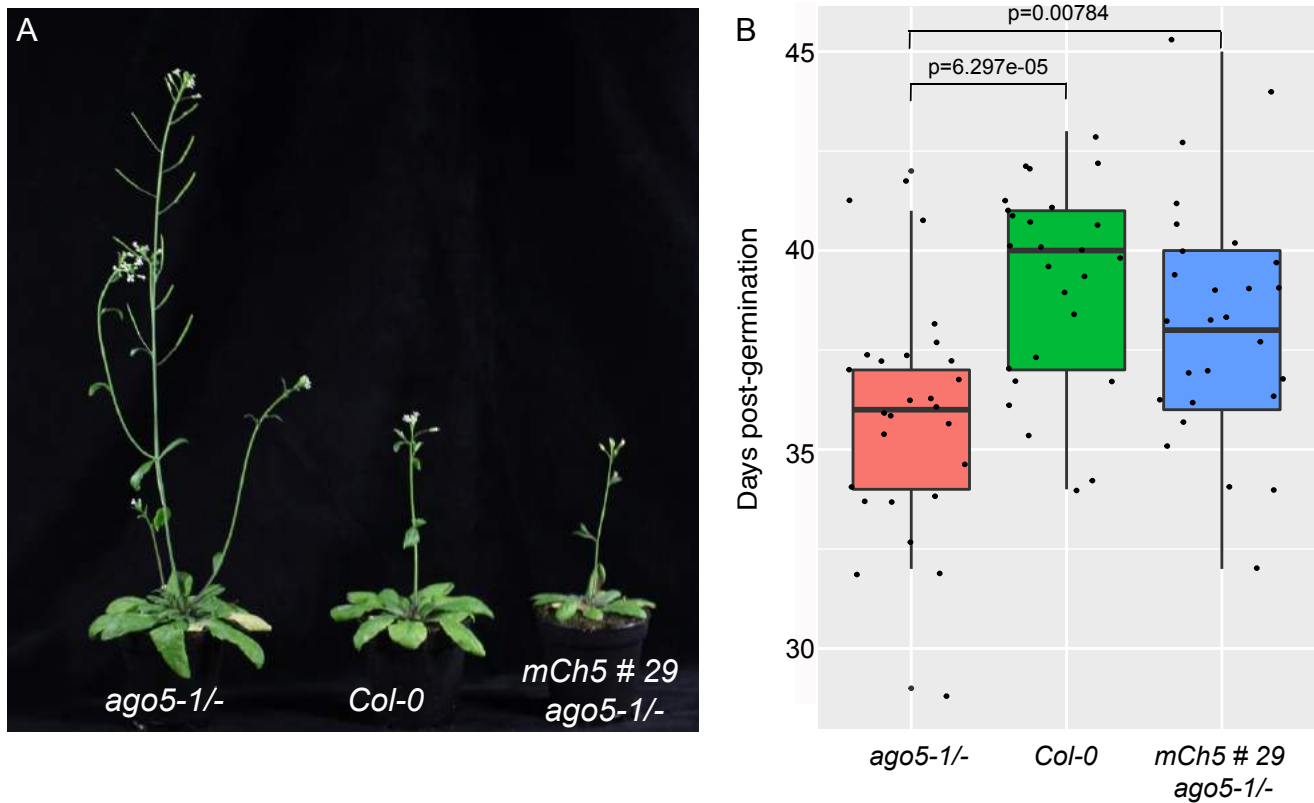


Fig. S4. Complementation of *ago5-1* mutant by pAGO5:mCherry-AGO5. (A) Illustrative pictures of the early flowering phenotype of *ago5-1/-* compared to *Col-0* and *mCh5 #29 ago5-1/-*. (B) Quantification of *ago5-1/-* flowering phenotype in *ago5-1/-* (n=27), *Col-0* (n=26) and *mCh5#29 ago5-1/-* (n=27).



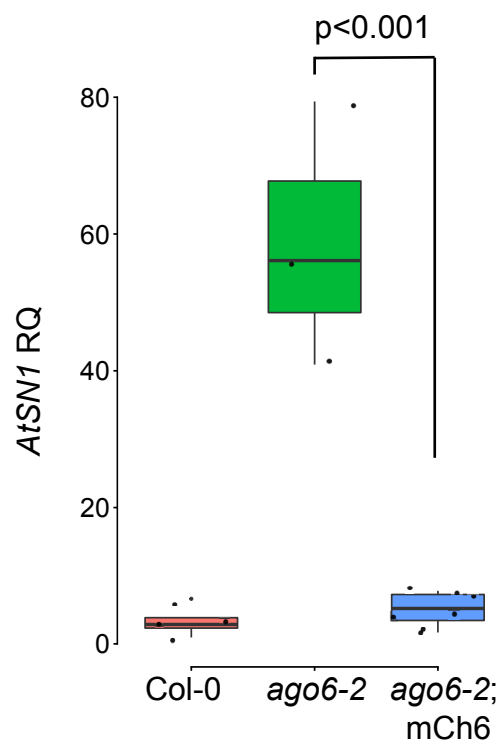


Fig. S5. Complementation of ago6-2 mutant by pAGO6:mCherry-AGO6. qPCR showing the absence of AtSN1 ectopic expression in rosette leaves of seven independent lines expressing the construct pAGO6:mCherry-AGO6 (mCh4) in ago6-2 background compared to Col-0 and ago6-2. Actin2 was used as endogenous control. p indicates the p value obtained by a Student's T-Test.

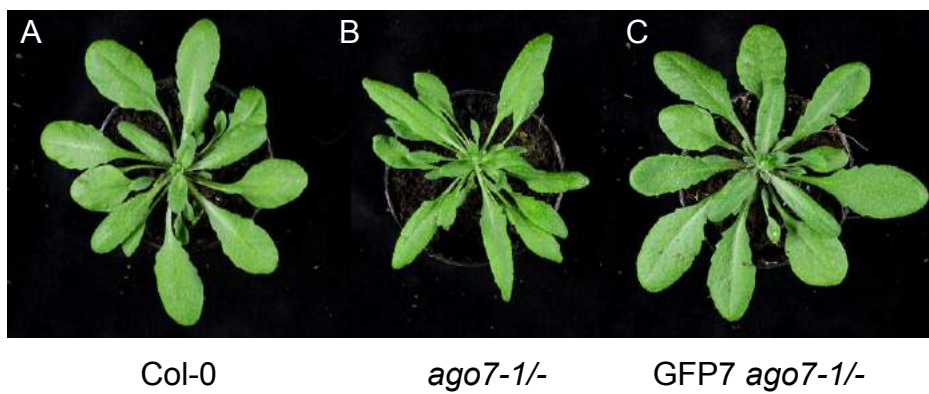


Fig. S6. Complementation of *ago7-1* mutant by pAGO7:GFP-AGO7. Illustrative pictures of the leaf phenotype of *ago7-1/-* (B) compared to Col-0 (A) and GFP-AGO7 *ago7-1/-* (C).

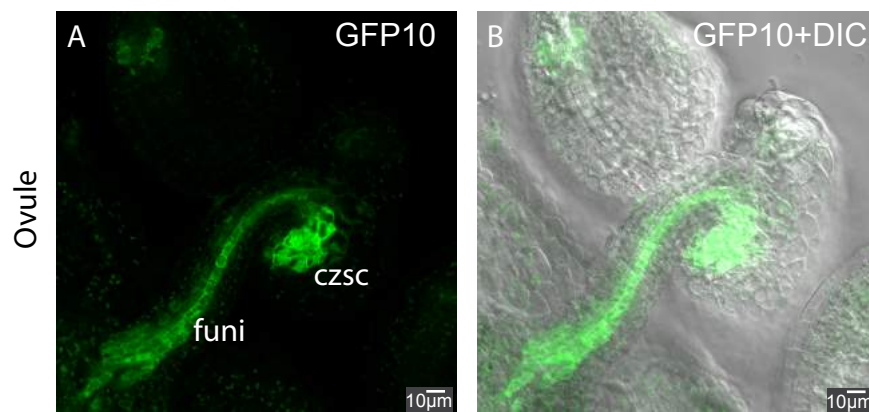


Fig. S7. Additional pictures of pAGO10:GFP-AGO10. (A-B) Picture representing the expression in ovules of GFP-AGO10 in the vascular tissue of the funiculus (funi) and at the vascular termination in the chalazal seed coat (czsc). Scale bars represent 10µm.

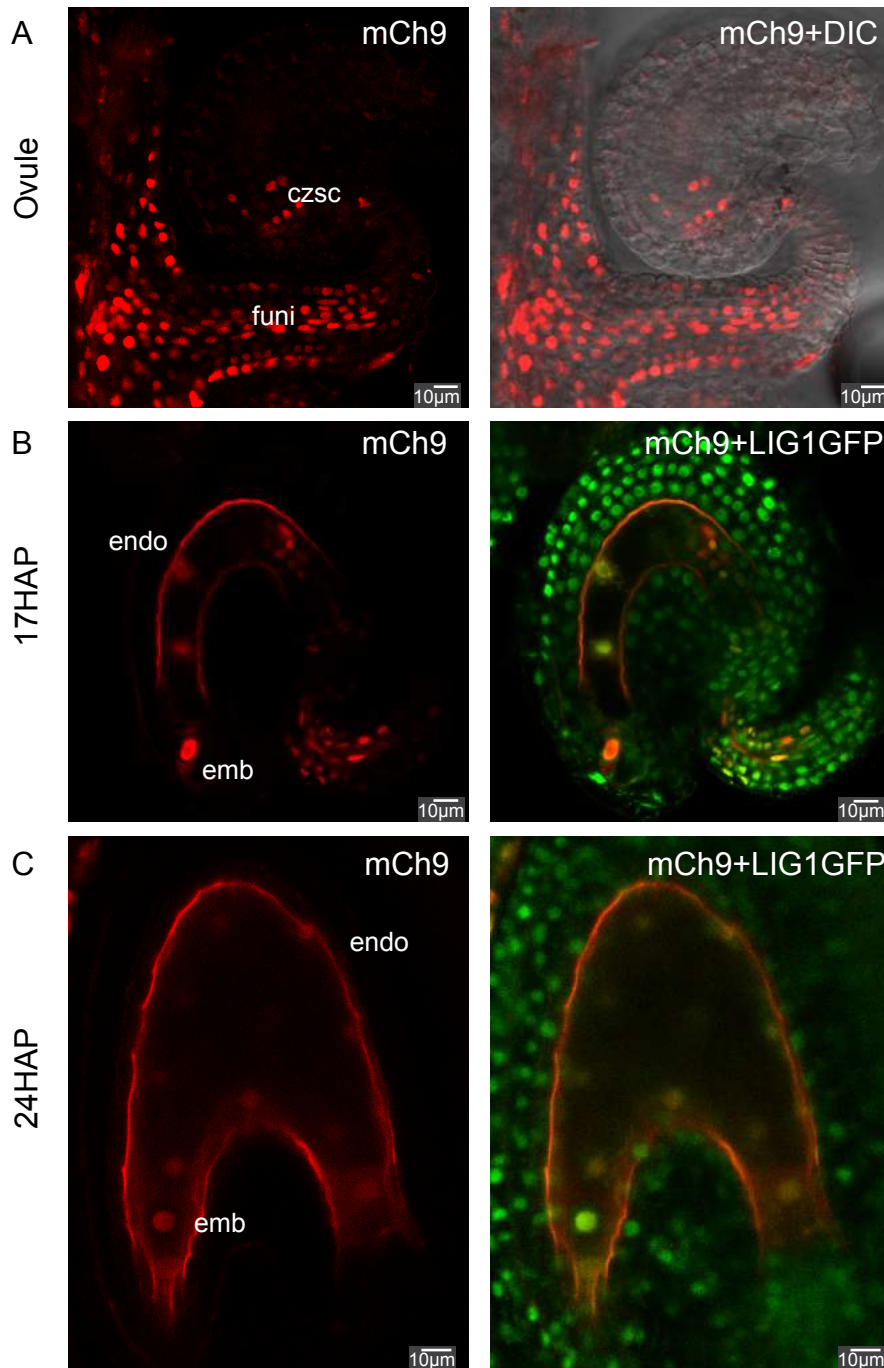
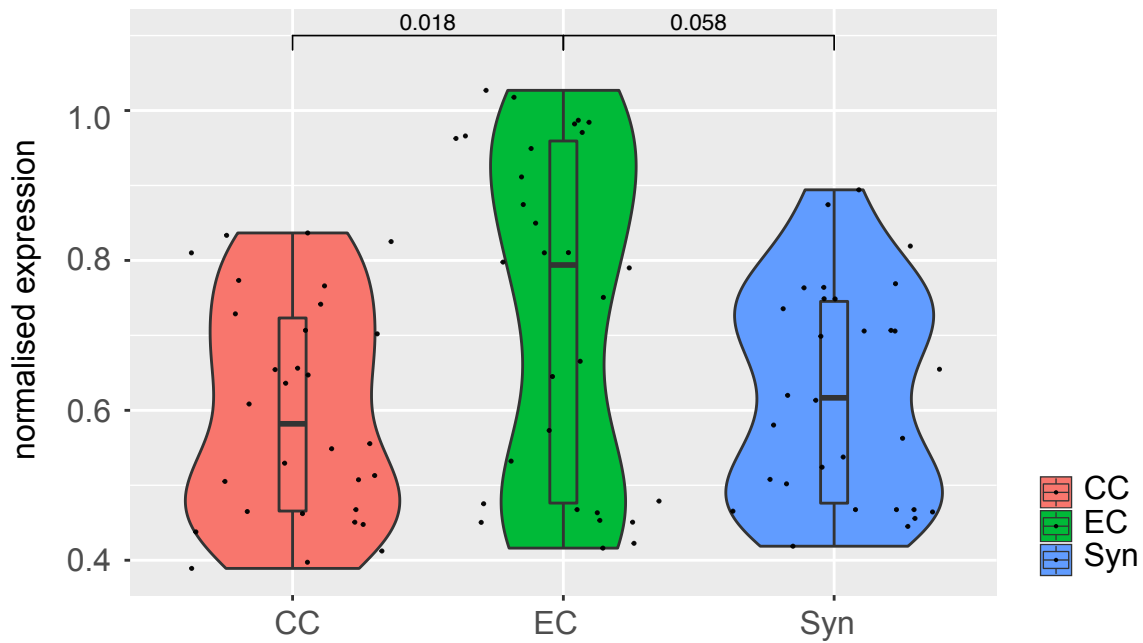


Fig. S8. Additional pictures of pAGO9:mCh-AGO9. (A) Pictures representing the expression in ovules of mCherry-AGO9 in the funiculus (funi) and in the chalazal seed coat (czsc). (B-C) Pictures representing the expression in developing seeds of mCh9 in early embryo and endosperm at 17 hours after pollination (HAP) (B) and at 24 HAP (C). Scale bars represent 10  $\mu\text{m}$ .

A



B

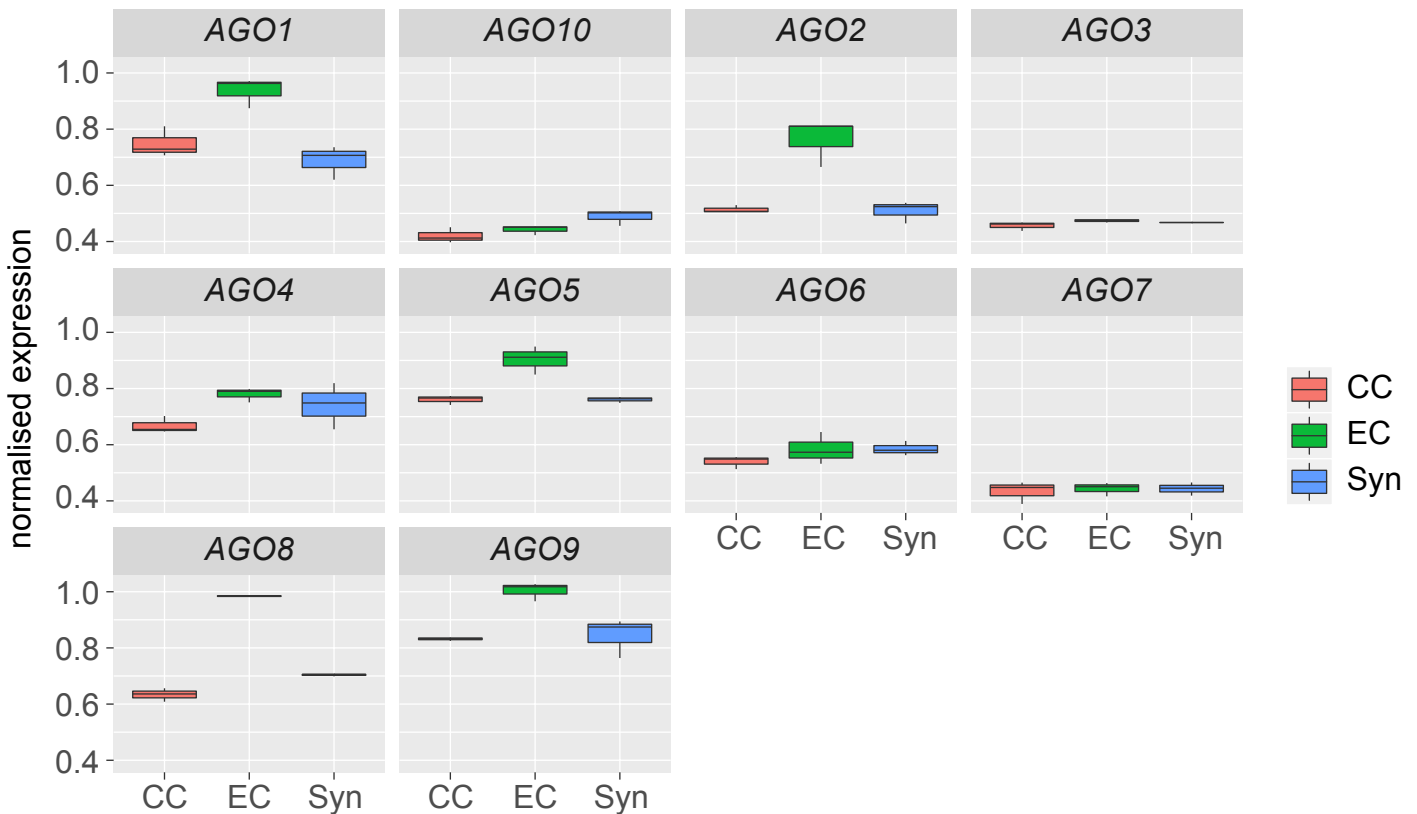
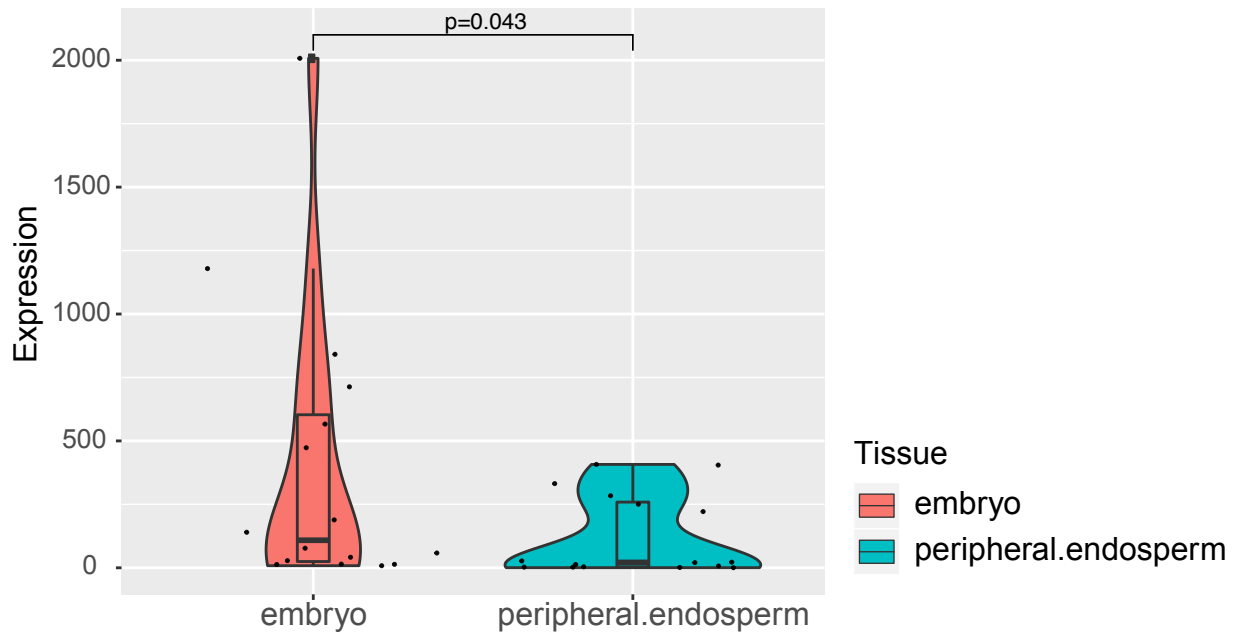


Fig. S9. Arabidopsis Argonautes expression extracted from microarray data of LCM dissected female gametophyte (Wuest et al, 2010) confirming the general enrichment of AGO transcript in the egg cell (EC) compared to central cell (CC) or synergids (Syn). (A) Violin plot representing the general enrichment of AGO expression in the EC. (B) AGOs individual expression boxplot in the different cell type. p values of a Wilcoxon test are indicated.

A



B

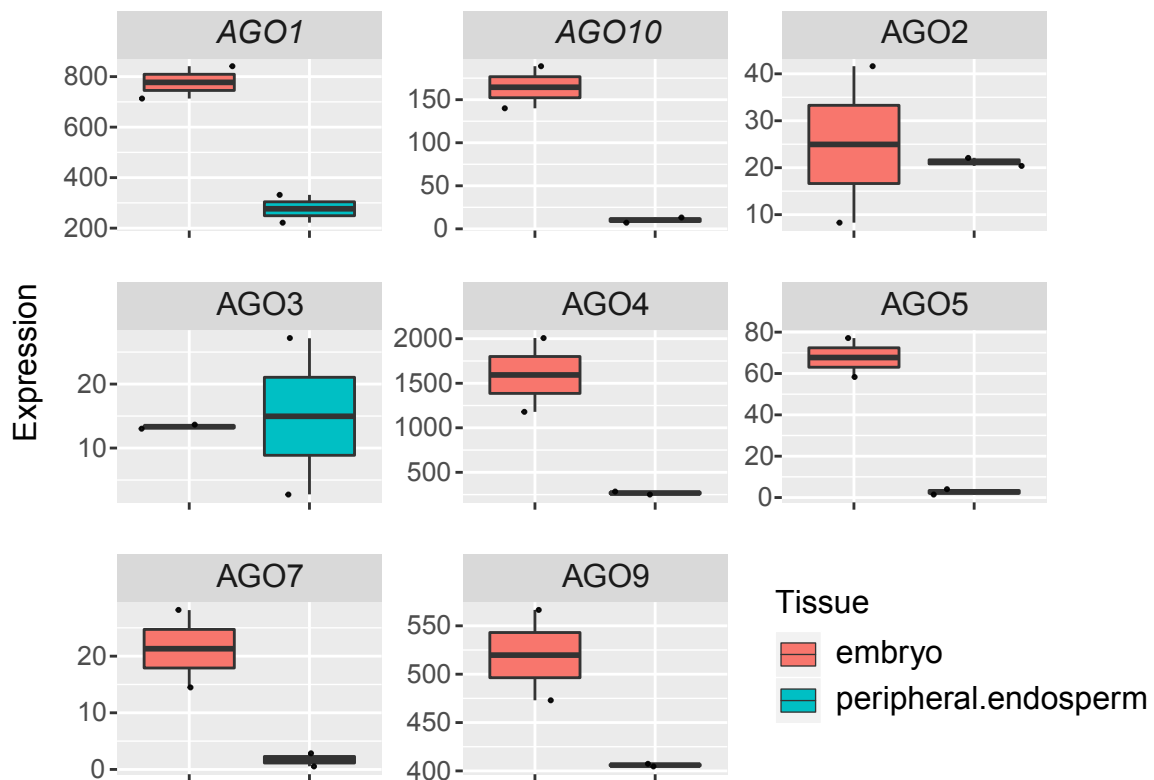


Fig. S10. Arabidopsis Argonautes expression extracted from microarray data of LCM dissected seeds at the pre-globular stage (Belmonte et al., 2013) confirming the general enrichment of AGO transcripts in the embryo compared to the peripheral endosperm. (A) Violin plot representing the general enrichment of AGOs expression in the embryo. (B) AGOs individual expression boxplot in the different cell type. p values of a Wilcoxon test are indicated. AGO6 and AGO8 probes are not present in these data.

	female gametophyte			male gametophyte		developping seed			sporophyte				
	ec	syn	cc	s	v	endo	emb	heart	nuc	ii	oi	czsc	fu
AGO1	expressed	not expressed	not expressed	expressed	not expressed	not expressed	expressed	expressed	strongly expressed	expressed	not expressed	strongly expressed	expressed
AGO5	expressed	not expressed	not expressed	expressed	expressed	not expressed	expressed	SAM	strongly expressed	expressed	not expressed	expressed	expressed
AGO10	not expressed	not expressed	not expressed	not expressed	not expressed	not expressed	expressed	expressed	not expressed	expressed	not expressed	strongly expressed	expressed
AGO4	expressed	expressed	expressed	expressed	not expressed	not expressed	expressed	expressed	strongly expressed	strongly expressed	strongly expressed	strongly expressed	expressed
AGO6	expressed	expressed	expressed	expressed	expressed	not expressed	expressed	expressed	expressed	expressed	expressed	expressed	expressed
AGO8	not expressed	not expressed	not expressed	not expressed	not expressed	not expressed	not expressed	not expressed	not expressed	not expressed	not expressed	not expressed	not expressed
AGO9	strongly expressed	expressed	expressed	expressed	not expressed	expressed	expressed	SAM	strongly expressed	not expressed	not expressed	expressed	expressed
AGO2	strongly expressed	not expressed	not expressed	expressed	not expressed	not expressed	not expressed	not expressed	not expressed	not expressed	not expressed	not expressed	not expressed
AGO3	not expressed	not expressed	not expressed	not expressed	not expressed	not expressed	not expressed	not expressed	not expressed	not expressed	not expressed	not expressed	strongly expressed
AGO7	strongly expressed	expressed	expressed	strongly expressed	not expressed	not expressed	expressed	SAM	expressed	strongly expressed	strongly expressed	strongly expressed	expressed

Legend :

- Not expressed
- strongly expressed
- expressed
- lightly expressed

Fig S11. Summary table of AGO's expression pattern in reproductive tissues.